Engineering Structures 223 (2020) 111111

Contents lists available at ScienceDirect

Engineering Structures

journal homepage: www.elsevier.com/locate/engstruct

Topology optimization of buildings subjected to stochastic base excitation

Fernando Gomez[a,*], Billie F. Spencer Jr.[a], Juan Carrion[b,c]

[a] Civil and Environmental Engineering, University of Illinois at Urbana-Champaign, 205 N Mathews Ave, MC-250, Urbana, IL 61801, USA
[b] Skidmore, Owings & Merrill, LLP, 224 S Michigan Ave # 1000, Chicago, IL, USA
[c] Department of Civil Engineering, University of Cuenca, Cuenca, Ecuador

ARTICLE INFO

Keywords:
Topology optimization
Seismic building design
Dynamic condensation
Stochastic dynamics
Minimax problem
Lyapunov equation

2010 MSC:
00-01
99-00

ABSTRACT

In seismically active regions, buildings are inevitably exposed to extreme ground motions. Traditionally, the main structural system is designed iteratively to resist these loads, which provides safe systems, but is usually suboptimal. Topology optimization provides an approach to obtain optimal material layout; however, most approaches only accommodate deterministic loads. Moreover, typical structural design goals require minimization of the maximum of some set of responses; such a goal is typically non-smooth, which impairs the use of efficient gradient-based optimizers. This study models the stochastic ground excitation as a zero-mean filtered white noise and combined with the model of the structure to form an augmented system. The structural response stationary covariances are obtained by solving a corresponding Lyapunov equation. The optimization problem is formulated to minimize the maximum structural response covariances, employing equivalent smooth formulations. Dynamic condensation is also employed to increase the efficiency. Sensitivities are computed by solving an adjoint Lyapunov equation, allowing for a gradient-based solver to be used. This study implements the following building features: additional discrete floor masses, boundary elements, and floor diaphragms. The proposed strategy is illustrated for seismically excited buildings with different properties. The results presented herein demonstrate the efficacy of this approach for efficient topology optimization of buildings subjected to stochastic ground motion.

1. Introduction

Effectively ensuring the seismic performance of structures is still one of the important problems in civil engineering. Current design procedures are based on an iterative process, which guarantees structural safety, but may not result in optimal structures [1]. Topology optimization provides a general approach to obtain optimal material layout in a prescribed structural domain according to some objective function and subjected to given design constraints [2]. Extensive research has been done in topology optimization to develop well-posed formulations [3–5] and solve inherent numerical problems such as mesh dependency, checkerboard patterning, islanding, local minima, etc. [6,5,7]. Topology optimization also has been applied to various dynamic problems in free vibration and forced vibration in general domains [2]. However, most of the published research on structural optimization only deals with deterministic loads. Such deterministic approaches cannot directly accommodate the stochastic dynamic loads which civil structures frequently experience (e. g., winds, earthquakes, traffic, etc.; see [8]), and therefore, produce suboptimal designs.

Seismic ground motion is one of the most severe loadings that civil structures experience. Although structures subjected to seismic excitation are typically designed and expected to undergo inelastic behavior, in most cases, the current design process assumes linear behavior of the structure and employs approximate methods such as the response spectrum method. For certain important structures, such as buildings with special response characteristic or special systems, for example buildings for hospitals or buildings with supplemental nonlinear devices, nonlinear time history analyses are conducted to more accurately verify the building behavior. In general, nonlinear analysis is not a design tool, as initial properties are required as input; however, it is used as a verification method. Thus, many researchers have considered linear analysis in structural optimization of seismically excited structures. For example, researchers have employed Monte Carlo Simulation to incorporate random excitation into the structural optimization problem. Balling et al. [9] conducted size optimization for buildings using Monte Carlo Simulation; this approach can be time prohibitive due to the large number of simulations required for convergence. Researchers in earthquake engineering have considered topology optimization for specific ground motion records [10], with each record being one realization of the underlying random process. Other approaches include

* Corresponding author.
E-mail addresses: gmzsnch2@illinois.edu (F. Gomez), bfs@illinois.edu (B.F. Spencer), juan.carrion@som.com (J. Carrion).

https://doi.org/10.1016/j.engstruct.2020.111111
Received 7 February 2020; Received in revised form 21 June 2020; Accepted 10 July 2020
Available online 04 August 2020

Nomenclature

$\mathbf{A}_a$	state space matrix of augmented system
$\mathbf{A}_{CP}$	state space for high-pass filtering in CP model
$\mathbf{A}_f$	state space matrix of excitation system
$a_{g(t)}$	ground acceleration
$\mathbf{A}_{KT}$	state space matrix for KT model
$\mathbf{A}_s$	state space matrix of structural system
$\mathbf{B}_a$	state space matrix of augmented system
$\mathbf{B}_{CP}$	state space for high-pass filtering in CP model
$\mathbf{B}_f$	state space matrix of excitation system
$\mathbf{B}_{KT}$	state space matrix for KT model
$\mathbf{B}_s$	state space matrix of structural system
$\mathbf{C}$	global damping matrix of the system
$\mathbf{C}_a$	state space matrix of augmented system
$\mathbf{C}_{CP}$	state space for high-pass filtering in CP model
$\mathbf{C}_f$	state space matrix of excitation system
$\mathbf{C}_{KT}$	state space matrix for KT model
$\mathbf{C}_s$	state space matrix of structural system
c_0	coefficient in modified SIMP for mass density
$\mathbf{D}_s$	state space matrix of structural system
$\mathbf{D}_{CP}$	state space for high-pass filtering in CP model
e	Normalized error of response using Guyan transformation
$E(z)$	Young's modulus using SIMP model
E^0	Young's modulus of solid material
$\mathbb{E}(\cdot)$	expected value operator
$\mathbf{F}$	symmetric positive semidefinite matrix used in objective function
$\mathbf{F}_i$	symmetric positive semidefinite matrix used in objective J_i
$\mathbf{G}$	load effect matrix
$\mathbf{I}_{i\times i}$	identity matrix of size $i \times i$
J	objective function
J_i	objective function i
$\overline{J_i}$	normalized objective function i
J_{KS}	KS objective function, approximates J_{max}
J_{SOV}	objective function that sums the variance of different responses
J_{max}	objective function that takes the maximum variance among different responses
J_0	normalization constant in KS function
$\mathbf{K}$	global stiffness matrix of the system
$\mathbf{l}$	vector with entries equal to 1 for lateral DOF and 0 otherwise
M	lumped mass at each floor and axis in example 1
$\mathbf{M}$	global mass matrix of the system
N	number of DOF of the system
n_1	number of DOF retained
N_1	number of states of the excitation system
N_{el}	number of elements in the optimization
N_f	number of floors
p	penalization factor of Young's modulus using SIMP
q	penalization factor of mass density using SIMP
R	linear hat filter radius
$\mathbf{S}$	constraint matrix
S	set of indices
S_0	magnitude of the two-sided constant power spectral density
$\mathbf{T}$	transformation matrix for Guyan reduction
$\mathbf{T}_a$	Guyan transformation matrix for displacement and velocity
$\mathbf{T}_c$	transformation matrix for structural constraint
$\mathbf{T}_2$	block of transformation matrix $\mathbf{T}$
t, t_i	time
$\mathbf{u}$	displacement vector, relative to the ground
$\bar{\mathbf{u}}$	displacement vector of master DOF
$\tilde{\mathbf{u}}$	displacement vector of retained DOF
$\mathbf{u}_c$	displacement vector of constrained DOF
$\mathbf{u}_r$	displacement vector of removed DOF
v	internal variable for the KT model
V_{max}	volume upper limit
$V(\mathbf{z})$	volume for a density vector $\mathbf{z}$
$w(t)$	white noise process, input to the excitation model
$\mathbf{x}_a$	state vector of augmented system
$\mathbf{x}_f$	state vector of excitation system
$\mathbf{x}_s$	state vector of structural system
$\mathbf{y}$	output responses of interest
$\mathbf{z}$	vector of relative densities
z_{min}	lower bound for density variables
z_{max}	upper bound for density variables
z_n	relative density of element n
α_1	mass matrix coefficient for Rayleigh damping
α_2	stiffness matrix coefficient for Rayleigh damping
β	additional variable in bound formulation
$\mathbf{\Gamma}$	covariance matrix of response using dynamic condensation in example 1
$\mathbf{\Gamma}_0$	covariance matrix of response of complete system
$\mathbf{\Gamma}_{\mathbf{x}_a}$	covariance matrix of stationary response
$\mathbf{\Gamma}_{\mathbf{y}}$	covariance matrix of stationary structural output
ϵ	Ersatz parameter
$\mathbf{\Lambda}_i$	adjoint variable to compute sensitivity for objective J_i
$\phi(\cdot,\cdot)$	continuous differentiable positive scalar function, objective function
μ	ratio of mass of retained DOF over mass of removed DOF
ν	Poisson's ratio
ω_f	cut-off frequency of the CP excitation model
ω_g	frequency of the excitation model
ρ	KS parameter
$\rho(z)$	mass density using SIMP model
ρ^0	mass density of solid material
ζ_f	damping ratio for the cut-off frequency of the CP excitation model
ζ_g	damping ratio of the excitation model
$\mathbf{0}_{i\times j}$	zero matrix of size $i \times j$
$\dot{\cdot}$	time derivative
$\ddot{\cdot}$	time second derivative
$\tilde{\cdot}$	matrix or vector of the reduced-order system
^{T}	transpose of matrix
$\|\cdot\|_F$	Frobenius norm of a matrix

time-domain solution of the reliability-based topology optimization of building-like structures with probability constraints [11], frequency-domain solutions based on the first few modes of the building-like structures to obtain the covariance of the displacement [12,13], and explicit time-domain solution to obtain the covariance [14]. Recently, [15] proposed a formulation for topology optimization of general structures subjected to stochastic dynamic loading, in which a large-scale Lyapunov equation was solved to obtain the covariance of the response. This method provides promising results in topology optimization of stochastically excited structures. However, the seismic design of buildings often requires the minimization of the maximum of several structural responses (e.g., minimization of the maximum interstory drift). Such design objectives result in min–max structural optimization problems, which are inherently non-smooth, hindering the use of gradient-based methods required for efficient topology optimization. To date, topology optimization approaches that can handle the min–max problem for stochastically excited structures have not been reported.

This paper proposes an efficient topology optimization framework for buildings subjected to stochastic ground motions. The stochastic ground excitation is modeled as a zero-mean filtered white noise; an augmented state space representation is formed by combining the equation of motion for the structure with the excitation filter. Then, the stationary covariances of the structural responses of interest are obtained by solving a large-scale Lyapunov equation. The optimization problem is formulated to minimize the maximum among the covariances of the structural responses of interest. Subsequently, this min–max problem is transformed to an equivalent smooth formulation. Because the response of only a few locations is of interest in many building applications (e.g., interstory drift), a Guyan reduction is applied to reduce the order of the system and increase computational efficiency. A gradient-based method is then used to update the design variables, while the sensitivities are computed using an efficient method that requires the solution of an adjoint Lyapunov equation. This paper is organized as follows: Section 2 describes the problem formulation including the state space representation of the structure and excitation, the response under stochastic excitation, building characteristics, and topology optimization formulation; Section 3 provides details for the solution of the optimization problem using an equivalent formulation for the minimax problem and incorporating dynamic condensation to obtain stochastic response, sensitivity analysis of the functions, and optimization details; to demonstrate the efficacy of the proposed approach, Section 4 shows numerical examples of the optimization of buildings subjected to stochastic ground motion with different properties; and Section 5 presents the conclusions of this work.

2. Problem formulation

This section presents the topology optimization problem for buildings subjected to stationary stochastic dynamic loading. The structural model is described, the excitation is modeled as a filtered white noise, and the covariance matrix of the stationary stochastic responses is obtained. This background is summarized here briefly for the convenience of the reader; further details are provided in Gomez and Spencer [15]. Finally, the topology optimization framework is presented based on this formulation.

2.1. Building characteristics

Typical buildings differ from other types of structures due to some unique features that will be described in this section. The topology optimization framework proposed in this study is tailored to consider these characteristics in order to provide more realistic examples. In addition, some characteristics as explained in the next section allow improvement in the efficiency of the method without losing accuracy.

Consider the typical building model shown in Fig. 1 subjected to seismic ground motion. One of the most important characteristics is that buildings are divided into N_f floors, not necessarily of the same height, and only the response of the floors is of interest to the designer. The focus of this study is to design the lateral resisting system (LRS), which is modeled as a continuous design domain and discretized using 4-node quadrilateral (Q4) finite elements. In addition, each floor contains structural elements such as slabs and floor framing that are not part of the LRS and non-structural elements such as finishes, partition walls, mechanical–electrical-plumbing (MEP) components, and permanent live loads. All these elements provide additional structural masses to the system and are not included in typical examples of topology optimization of buildings. Moreover, this additional mass is typically higher than the mass of the lateral resisting system; values larger than 10 are typical in buildings subjected to ground motions; for example, a well-known benchmark problem consisting of a 9-story building subjected to seismic excitation yield a value of 21 [16]. Even larger values of the mass ratio of additional elements to the LRS elements are possible, e.g., more than 100, when a small part of the frames belong to LRS and the rest of frames belong to the gravity resisting system. In stochastic dynamics problems, these masses are extremely important because they modify the structural dynamic properties, which ultimately affects the stochastic building responses. The additional masses can be modeled as lumped masses in some floor nodes or distributed among all nodes in the floor. Fig. 1 shows the additional lumped masses as small filled red circles.

Another feature of buildings is that besides the LRS, the structure

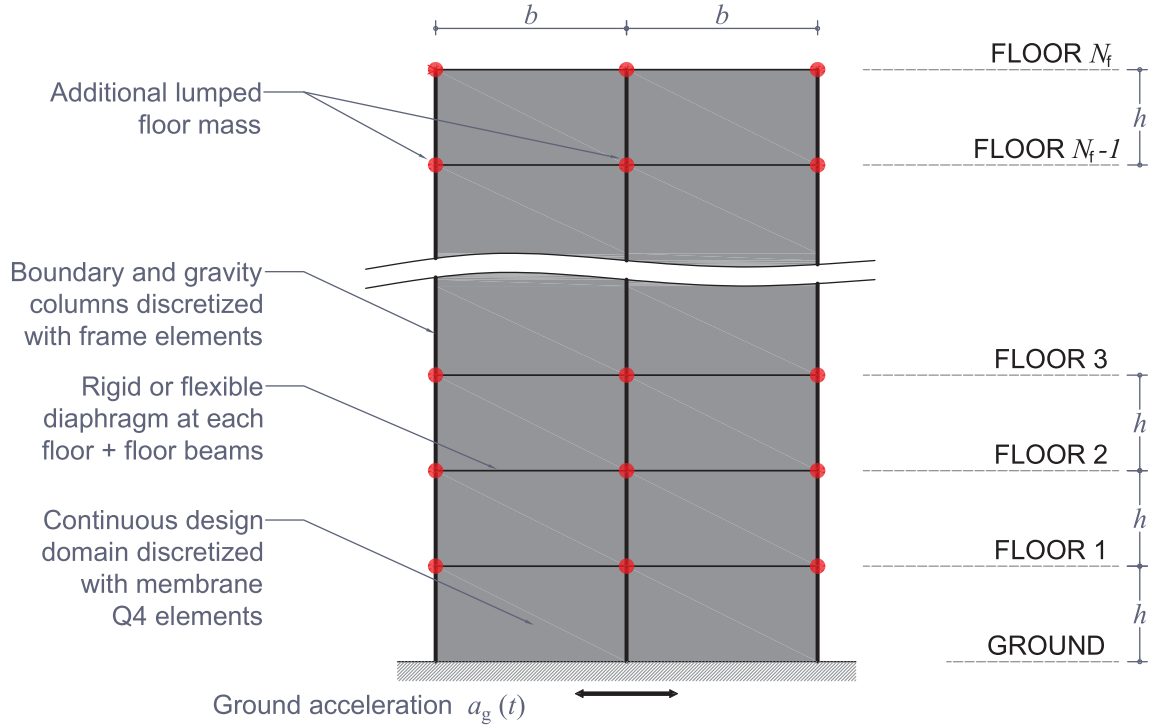

Fig. 1. Schematic of building subjected to ground motions.

has a gravitational resisting system, and some elements belong to both, especially in the boundary between both systems. For example, there exist boundary columns in the LRS, which support gravitational and lateral loads. In examples of topology optimization of buildings available in the literature, elements that support vertical axial loads due to overturning moments naturally appear along the boundary [17]. However, column-like elements might account for a large portion of the domain and constrained volume, therefore limiting the bracing patterns; furthermore, because of their dimensions, large vertical elements along the boundary will also have rather large flexural stiffness, which is not realistic of actual discrete structural elements in buildings. Consequently, it is preferable to include boundary columns to obtain cleaner bracing patterns in the LRS [17] as wells as bracing systems dominated by axial behavior. The boundary elements can be modeled as frame elements, which present translational and rotational degrees of freedom, such that the end nodes of the frame elements match with the nodes of the continuous elements in the optimization domain; also, there is no need to enrich continuous elements with drilling degrees-of-freedom (DOF) to match the rotational DOF of the frame elements [17]. Similarly, beams can be included by using frame elements with end nodes coinciding with the nodes of the continuous elements in the design domain. However, in this type of structures, beam elements serve mainly as elements for gravity loads and provide some flexural stiffness when a rigid diaphragm is included, and in the case of a flexible diaphragm, they provide some axial and flexural stiffness.

Another important detail of buildings is that the floor system that supports gravitational loads, also acts as a diaphragm to distribute lateral loads. Two types of diaphragms are considered in this study: rigid and flexible. A rigid diaphragm possesses infinite axial stiffness and imposes the same lateral displacement in all floor nodes. A flexible diaphragm uses the actual axial stiffness of the floor system. Rigid diaphragms are implemented by applying constraints to the displacements; further details on the implementation of the rigid diaphragm are shown in 3.2. Rigid diaphragms are a good approximation for lateral resisting frame systems with thick concrete slabs. In braced frame systems, flexible diaphragms may be preferred for the analysis and design. In these systems, the rigid diaphragm assumption may provide an unrealistically high axial stiffness and eliminate the horizontal component of the brace forces, that should be resisted by other members of the system (e.g., horizontal struts and ties). Furthermore, in steel bracing systems, it is difficult and typically undesired to transfer large forces from the steel members to the concrete slab (so that the diaphragm can be engaged) and then back to the steel member.

2.2. Structural model

Using standard finite element methods, the domains are discretized and 2D translational DOF are assigned to the Q4 elements, and 2D translational and rotational DOF are assigned to the frame elements. The mass and stiffness matrix and loading vector for each element is computed, and the global mass and stiffness matrices and the loading vector are assembled. The only type of damping included is intrinsic building damping, and the damping matrix is computed from the global mass and stiffness matrices using specific damping ratios.

The standard equation of motion of a dynamic linear building with N DOF is satisfied and it is given by

$$\mathbf{M}\ddot{\mathbf{u}} + \mathbf{C}\dot{\mathbf{u}} + \mathbf{K}\mathbf{u} = \mathbf{G}a_g(t) \tag{1}$$

where $\mathbf{M}$, $\mathbf{C}$, and $\mathbf{K}$ represent the mass, damping, and stiffness matrices, respectively; $\mathbf{G}$ is the load effect matrix and for ground motions $\mathbf{G} = -\mathbf{M}\mathbf{l}$ where $\mathbf{l}$ is a vector with entries equal to 1 for lateral DOF and 0 otherwise; $a_g(t)$ is the input excitation, i.e., scalar ground motion acceleration; and $\mathbf{u}$ is the displacement vector.

Defining the vector $\mathbf{x}_s$ as

$$\mathbf{x}_s = [\mathbf{u}^T \quad \dot{\mathbf{u}}^T]^T \tag{2}$$

the system can be represented in the state space form by

$$\begin{aligned}\dot{\mathbf{x}}_s &= \mathbf{A}_s\mathbf{x}_s + \mathbf{B}_s a_g(t)\\ \mathbf{y} &= \mathbf{C}_s\mathbf{x}_s + \mathbf{D}_s a_g(t)\end{aligned} \tag{3}$$

where the state matrices $\mathbf{A}_s$ and $\mathbf{B}_s$ are

$$\mathbf{A}_s = \begin{bmatrix} \mathbf{0}_{N\times N} & \mathbf{I}_{N\times N} \\ -\mathbf{M}^{-1}\mathbf{K} & -\mathbf{M}^{-1}\mathbf{C} \end{bmatrix}, \quad \mathbf{B}_s = \begin{bmatrix} \mathbf{0}_{N\times 1} \\ \mathbf{M}^{-1}\mathbf{G} \end{bmatrix} \tag{4}$$

with $\mathbf{0}$ is a matrix of zeros, and $\mathbf{I}$ is the identity matrix, both with dimensions given by the subscripts; $\mathbf{y}$ is the vector of output responses of interest corresponding to the matrices $\mathbf{C}_s$ and $\mathbf{D}_s$.

2.3. Stochastic ground motion

Ground motions behave as non-stationary stochastic scalar processes, which can be modeled as the product of a stationary process and a slowly varying envelope function; moreover, a typical earthquake record consists of three phases: an initial buildup phase, a stationary strong-motion portion, and decaying tail [8]. For many earthquakes, the strong-motion portion is long, such that the structure will achieve peak structural response in this portion, therefore, modeling the ground motion as a stationary process is a good approximation [8]. It is worth noting that when the ground motion contains large impulsive components, such as near-source earthquakes, a non-stationary stochastic process model is more accurate; although, the stationary assumption yields a conservative design.

A typical model for the strong-motion of ground acceleration $a_g(t)$ is given by the Kanai-Tajimi (KT) model [18] whose differential equation is

$$\begin{aligned}\ddot{v} + 2\zeta_g\omega_g\dot{v} + \omega_g^2 v &= w(t)\\ a_g(t) &= -2\zeta_g\omega_g\dot{v} - \omega_g^2 v\end{aligned} \tag{5}$$

where v is the internal variable for the KT model, ω_g and ζ_g are the frequency and damping ratio of the excitation and they are determined by the characteristics of the local earth surface layer, and $w(t)$ is a scalar white noise process that satisfies

$$\mathbb{E}(w(t)) = 0, \quad \mathbb{E}(w(t_1)w(t_2)) = 2\pi S_0\delta(t_1 - t_2) \tag{6}$$

where $\mathbb{E}(\cdot)$ is the expected value operator, S_0 is the magnitude of the two-sided constant power spectral density, and $\delta(\cdot)$ is the Dirac delta function. The parameters can be estimated from local ground motion records using statistical estimators and the intensity S_0 of the excitation is given by the intensity of the ground motion.

From the differential equations, the state space representation can be easily obtained. Therefore, in general the stochastic ground motion is modeled as a filtered white-noise with the following space state space representation

$$\begin{aligned}\dot{\mathbf{x}}_f &= \mathbf{A}_f\mathbf{x}_f + \mathbf{B}_f w(t)\\ a_g(t) &= \mathbf{C}_f\mathbf{x}_f\end{aligned} \tag{7}$$

where the matrices $\mathbf{A}_f$, $\mathbf{B}_f$, and $\mathbf{C}_f$ are based on the characteristics of the excitation; $\mathbf{x}_f$ is the state vector of the excitation model with N_1 states; and $w(t)$ is a scalar white noise process.

For example, for the KT model, the state vector is defined as

$$\mathbf{x}_f = [v \quad \dot{v}]^T \tag{8}$$

then, the space state matrices are given by

$$\begin{aligned}\mathbf{A}_f = \mathbf{A}_{KT} &= \begin{bmatrix} 0 & 1 \\ -\omega_g^2 & -2\omega_g\zeta_g \end{bmatrix}, \quad \mathbf{B}_f = \mathbf{B}_{KT} = \begin{bmatrix} 0 \\ 1 \end{bmatrix},\\ \mathbf{C}_f = \mathbf{C}_{KT} &= [-\omega_g^2 \quad -2\omega_g\zeta_g]\end{aligned} \tag{9}$$

The previous model has a non-zero power spectral density (PSD) at zero frequency, which is not realistic for acceleration records. The previous model can be corrected by applying a high-pass filter, for example, the

Clough-Penzien model [19] whose space state matrices are

$$\mathbf{A}_{\mathrm{f}} = \begin{bmatrix} \mathbf{A}_{\mathrm{KT}} & \mathbf{0}_{2\times 2} \\ \mathbf{B}_{\mathrm{CP}}\mathbf{C}_{\mathrm{KT}} & \mathbf{A}_{\mathrm{CP}} \end{bmatrix}, \quad \mathbf{B}_{\mathrm{f}} = \begin{bmatrix} \mathbf{B}_{\mathrm{KT}} \\ \mathbf{0}_{2\times 1} \end{bmatrix}, \quad \mathbf{C}_{\mathrm{f}} = [\mathbf{D}_{\mathrm{CP}}\mathbf{C}_{\mathrm{KT}} \quad \mathbf{C}_{\mathrm{CP}}] \tag{10}$$

where $\mathbf{A}_{\mathrm{KT}}$, $\mathbf{B}_{\mathrm{KT}}$, $\mathbf{C}_{\mathrm{KT}}$are the state matrices of the Kanai-Tajimi model shown previously, and

$$\mathbf{A}_{\mathrm{CP}} = \begin{bmatrix} 0 & 1 \\ -\omega_{\mathrm{f}}^2 & -2\omega_{\mathrm{f}}\zeta_{\mathrm{f}} \end{bmatrix}, \quad \mathbf{B}_{\mathrm{CP}} = \begin{bmatrix} 0 \\ 1 \end{bmatrix},$$
$$\mathbf{C}_{\mathrm{CP}} = [-\omega_{\mathrm{f}}^2 \quad -2\omega_{\mathrm{f}}\zeta_{\mathrm{f}}], \quad \mathbf{D}_{\mathrm{CP}} = [1] \tag{11}$$

where ω_{f} and ζ_{f} are the frequency and damping ratio of a single DOF system to filter low frequencies. Typically, $\omega_{\mathrm{f}} \ll \omega_{\mathrm{g}}$ and $\zeta_{\mathrm{f}} \geqslant \zeta_{\mathrm{g}}$ [19].

The difference between the two models of ground motion is evident only in the lower frequencies. This fact is demonstrated by Fig. 2, which shows the frequency response functions of both models using $\omega_{\mathrm{g}} = 20$ rad/s, $\zeta_{\mathrm{g}} = 0.30$, $\omega_{\mathrm{f}} = 2$ rad/s, and $\zeta_{\mathrm{g}} = 0.70$. Furthermore, the stochastic response is related to the area under the curve of the PSD curve, therefore, the difference between responses using both models is only relevant when the first frequency of the structure is much smaller than ω_{g}.

2.4. Stochastic structural responses

Given the structural and excitation models, the augmented state vector $\mathbf{x}_{\mathrm{a}}$ can be defined as

$$\mathbf{x}_{\mathrm{a}} = [\mathbf{x}_{\mathrm{s}}^{\mathrm{T}} \quad \mathbf{x}_{\mathrm{f}}^{\mathrm{T}}]^{\mathrm{T}} \tag{12}$$

yielding an augmented system whose state space representation is given by

$$\dot{\mathbf{x}}_{\mathrm{a}} = \mathbf{A}_{\mathrm{a}}\mathbf{x}_{\mathrm{a}} + \mathbf{B}_{\mathrm{a}}\mathbf{w}(t)$$
$$\mathbf{y} = \mathbf{C}_{\mathbf{a}}\mathbf{x}_{\mathbf{a}} \tag{13}$$

where the matrices $\mathbf{A}_{\mathrm{a}}$, $\mathbf{B}_{\mathrm{a}}$, and $\mathbf{C}_{\mathrm{a}}$ are given by

$$\mathbf{A}_{\mathrm{a}} = \begin{bmatrix} \mathbf{A}_{\mathrm{s}} & \mathbf{B}_{\mathrm{s}}\mathbf{C}_{\mathrm{f}} \\ \mathbf{0}_{N_1\times N} & \mathbf{A}_{\mathrm{f}} \end{bmatrix}, \quad \mathbf{B}_{\mathrm{a}} = \begin{bmatrix} \mathbf{0}_{2N\times 1} \\ \mathbf{B}_{\mathrm{f}} \end{bmatrix}, \quad \mathbf{C}_{\mathrm{a}} = [\mathbf{C}_{\mathrm{s}} \quad \mathbf{D}_{\mathrm{s}}\mathbf{C}_{\mathrm{f}}] \tag{14}$$

The time history of the covariance matrix can be obtained solving a differential equation. However, because the ground excitation is assumed stationary, the stationary response achieves the maximum values of the response and it is the only value of interest. The covariance matrix $\mathbf{\Gamma}_{\mathbf{x}_{\mathrm{a}}}$ of the stationary response can be obtained by solving the Lyapunov equation

$$\mathbf{A}_{\mathrm{a}}\mathbf{\Gamma}_{\mathbf{x}_{\mathrm{a}}} + \mathbf{\Gamma}_{\mathbf{x}_{\mathrm{a}}}\mathbf{A}_{\mathrm{a}}^{\mathrm{T}} + 2\pi\mathbf{B}_{\mathrm{a}}\mathbf{S}_0\mathbf{B}_{\mathrm{a}}^{\mathrm{T}} = \mathbf{0} \tag{15}$$

Finally, the covariance of the structural output $\mathbf{y}$ can be calculated via

$$\mathbf{\Gamma}_y = \mathbb{E}(\mathbf{y}\mathbf{y}^{\mathrm{T}}) = \mathbf{C}_{\mathrm{a}}\mathbb{E}(\mathbf{x}_{\mathrm{a}}\mathbf{x}_{\mathrm{a}}^{\mathrm{T}})\mathbf{C}_{\mathrm{a}}^{\mathrm{T}} = \mathbf{C}_{\mathrm{a}}\mathbf{\Gamma}_{\mathbf{x}_{\mathrm{a}}}\mathbf{C}_{\mathrm{a}}^{\mathrm{T}} \tag{16}$$

2.5. Topology optimization formulation

The design variables in continuous-domain topology optimization are chosen as the relative density in each element [2]. Therefore for element n, the relative density variable is denoted by z_n, where $n \in \{1, 2, \ldots, N_{\mathrm{el}}\}$, and N_{el} is the total number of elements. The optimization formulation is thus given by:

Find $\mathbf{z} = [z_1, z_2, \ldots, z_{N_{\mathrm{el}}}]$ such that:

$$\begin{aligned} \min_{\mathbf{z}} \quad & J(\mathbf{z}) = \phi(\mathbf{\Gamma}_{\mathbf{x}_{\mathrm{a}}}(\mathbf{z}), \mathbf{z}) \\ \text{s. t.} \quad & g(\mathbf{z}) = V(\mathbf{z}) - V_{\max} \leqslant 0 \\ & \mathbf{A}_{\mathrm{a}}\mathbf{\Gamma}_{\mathbf{x}_{\mathrm{a}}} + \mathbf{\Gamma}_{\mathbf{x}_{\mathrm{a}}}\mathbf{A}_{\mathrm{a}}^{\mathrm{T}} + 2\pi\mathbf{B}_{\mathrm{a}}\mathbf{S}_0\mathbf{B}_{\mathrm{a}}^{\mathrm{T}} = \mathbf{0} \\ & z_n \in [z_{\min}, z_{\max}] \text{for} n = 1, 2, \ldots, N_{\mathrm{el}} \end{aligned} \tag{17}$$

where $\phi$is a continuous differentiable positive scalar function, $\mathbf{\Gamma}_{\mathbf{x}_{\mathrm{a}}}$ is the stationary covariance of the response, V is the volume of the structural system, $V_{\max}$ is the volume constraint, and $z_{\min}$ and $z_{\max}$ are the lower and upper bounds on the density variables.

The proposed performance function allows consideration of many different problems. For example, the following case represents the sum of variance (SOV) of the response of one or many DOFs

$$J_{\mathrm{sov}}(\mathbf{z}) = \mathbf{F}(\mathbf{z}) : \mathbf{\Gamma}_{\mathbf{x}_{\mathrm{a}}}(\mathbf{z}) \tag{18}$$

where $J_{\mathrm{sum}}(\mathbf{z})$ is the SOV objective function, : represents the sum of the diagonal entries of the product of matrices, and $\mathbf{F}$ is a symmetric positive semidefinite matrix. The objective function in Eq. (18) can represent the sum of variances of different types of response [15].

Typically, only the response at the floors is relevant in building design and the response of other points inside the design domain is rarely considered. For example, common response quantities in building design are roof displacement, interstory drifts, (i.e., relative lateral displacement between consecutive floors), and floor accelerations. In this study, the goal is to minimize the interstory drifts because they are related with non-structural and structural damage in the corresponding story, and therefore, it represents a safety limit state, which usually governs the structural design. In addition, because the input is a zero-mean stationary Gaussian stochastic process, interstory drifts are zero-mean stationary Gaussian stochastic processes. Furthermore, the marginal probability distribution of the interstory drift is fully characterized by the interstory drift variance, and therefore, minimizing the variance effectively minimizes the values of the corresponding stochastic process.

Although the sum of variances of floor responses is an interesting quantity, the actual goal in practice is to minimize the maximum response among all floors; minimizing the sum of variances is an indirect approach to minimize the maximum variance but they are not equivalent in all cases. Therefore, the following objective represent the maximum response among all floors

$$J_{\max}(\mathbf{z}) = \max_{i\in S}\left\{J_i(\mathbf{z})\right\} = \max_{i\in S}\left\{\mathbf{F}_i(\mathbf{z}) : \mathbf{\Gamma}_{\mathbf{x}_{\mathrm{a}}}(\mathbf{z})\right\} \tag{19}$$

where $J_{\max}(\mathbf{z})$ is the maximum (MAX) response objective function, S is set of indices, $J_i(\mathbf{z})$ is a response of interest, and $\mathbf{F}_i$ is a symmetric positive semidefinite matrix for $i \in S$. For example, for the maximum interstory drift of a building with N_{f} stories, $S = \{1, 2, \ldots, N_{\mathrm{f}}\}$ and $J_i(\mathbf{z})$ is the variance of the interstory drift of the i^{th} story. The function $J_{\max}$ is not a particular case of the function ϕ only because the former is not differentiable. Moreover, $J_{\max}$ is not differentiable close to the design point, which presents challenges in the numerical implementation.

As illustrated here, the performance function is completely defined

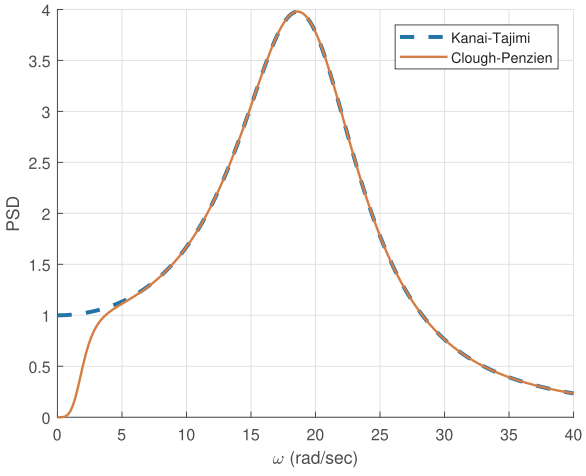

Fig. 2. PSD curves of Kanai-Tajimi and Clough-Penzien models.

by the covariance of the response $\mathbf{\Gamma}_{\mathbf{x}_a}$, which is obtained through solution of the Lyapunov equation. Consequently, the stochastic optimization problem has been transformed into a deterministic counterpart.

A gradient-based procedure is preferred for general optimization problems, such as the method of moving asymptotes [20], for which the gradient of the performance function and constraints are also required. While previous formulations were very general, efficient methods have not been developed that can handle minimax problems of topology optimization of buildings with stochastic ground excitation. The next section proposes means to overcome these problems.

3. Solution method

This section describes the proposed solution of the topology optimization framework using dynamic condensation to improve numerical efficiency of the solution. First, the solution to the minimax formulation is presented. Then, the dynamic condensation is described. Later, the evaluation of the sensitivities using dynamic condensation is presented.

3.1. Minimax equivalent formulation

The objective function $J_{\max}(\mathbf{z})$ is the maximum response objective function, over different functions $J_i(\mathbf{z})$ with $i \in S$. For example, it could represent the maximum interstory drift or the maximum floor acceleration of a building with N_f stories. The function $J_{\max}(\mathbf{z})$ is an envelope of all functions considered, and it is clearly continuous because all the functions J_i are continuous; however, the MAX function is not differentiable at all points. Fig. 3 shows an example of the variance of interstory drifts of two floors versus a parameter, which defines the stiffness of the first floor, of a two-story building, and it also shows the maximum function, which has a singularity when the envelope switches from one objective to the other. Moreover, the singularity is the point of interest because it minimizes the maximum function. This figure exemplifies a typical case in optimization of envelope functions, in which the critical points do not have derivative; therefore, the problem cannot be solved by simply choosing a small enough domain where the function is differentiable.

To overcome the non-smoothness of the MAX objective function, an alternative bound formulation is introduced. This bound formulation has been used in structural optimization with many loads and one objective for each load [21]. This alternative formulation introduces a new design variable β, which is also the new objective function and constraints all the functions J_i to be smaller than β. It can be shown that both problems have the same minimum if a unique global minimum exists, but the second formulation have the advantage that the objective function and the constraint functions are all smooth.

The alternative formulation for the MAX function is given by:

Find $\mathbf{z} = [z_1, z_2, ..., z_{N_{el}}]$ such that:

$$\begin{aligned} \min_{\mathbf{z},\beta} \quad & \beta \\ \text{s. t.} \quad & J_i(\mathbf{z}) - \beta \leqslant 0 \quad \text{for} i \in S \\ & g(\mathbf{z}) = V(\mathbf{z}) - V_{\max} \leqslant 0 \\ & \mathbf{A}_a \mathbf{\Gamma}_{\mathbf{x}_a} + \mathbf{\Gamma}_{\mathbf{x}_a} \mathbf{A}_a^T + 2\pi \mathbf{B}_a \mathbf{S}_0 \mathbf{B}_a^T = \mathbf{0} \\ & z_n \in [z_{\min}, z_{\max}] \text{for} n = 1, 2, ..., N_{el} \end{aligned} \tag{20}$$

Note that the number of variables is increased by one, which is negligible compared to the number of variables in topology optimization. The new objective function is linear, so computing the function and its sensitivities is straightforward. On the other hand, the number of nonlinear constraints is increased by the number of elements in S, and evaluation of the constraints is done directly once the covariance matrix is obtained. However, the computations of the gradients of the new constraints is not straightforward, and Section 3.3 presents the details to obtain these gradients efficiently. Note that the proposed approach to handle minimax problems requires more solutions of the Lyapunov equation. To make this approach better suited, a more computationally efficient approach is required, as will be described in later sections.

Another approach to solve the min–max problem is to substitute the original envelope or maximum function by the Kreisselmeier-Steinhauser (KS) function, which has been used for problems with multiple load cases [22]. First, each objective function is normalized as follows

$$\overline{J}_i = \frac{J_i}{J_0} - 1 \tag{21}$$

where J_0 is a constant chosen such that the normalized values are close to zero. Then, the KS function is defined as

$$J_{KS}\left(\mathbf{z}, \rho\right) = J_0 \left[1 + \frac{1}{\rho} \ln\left(\sum_{i=1}^{N_f} e^{\rho \overline{J}_i}\right)\right] \tag{22}$$

where ρ is a constant. Clearly, the new function J_{KS} is smooth because it is the composition of smooth functions. Moreover, the function J_{KS} is larger than the maximum value $J_{\max}$, and the function J_{KS} converges to $J_{\max}$ as ρ goes to infinity. The normalization allows to control numerical overflow and defines the constant ρ as dimensionless.

A continuation approach is chosen for both constants, i.e. their values are changed incrementally. The constant J_0 is chosen close to the maximum and it is updated every certain number of iterations. The constant ρ is increased every certain number of iterations from 1 to a large value. However, choosing very large values for ρ can cause unstable convergence due to numerical error. Another approach is to solve sequential problems with increasing values of ρ. Note that the number of variables or constraints is not increased as in the previous approach. In this study, both methods will be used and compared, to get a solution of the minimax problem.

3.2. Stochastic response using dynamic condensation

This section presents a dynamic condensation approach to improve the computational efficiency of the proposed methodology. In many problems of interest in structural engineering, there are elements that are not part of the optimization domain, for example: floor systems in the optimization of the lateral resisting system of a building, bridge deck in the optimization of bridge structures, engine in the optimization of the framing of a vehicle, etc. Moreover, these elements provide additional mass to the system that is typically larger than the structural system mass, and the amount of these additional elements is small compared to the number of DOF of the system. In the topology optimization scheme, the additional masses could be added using passive

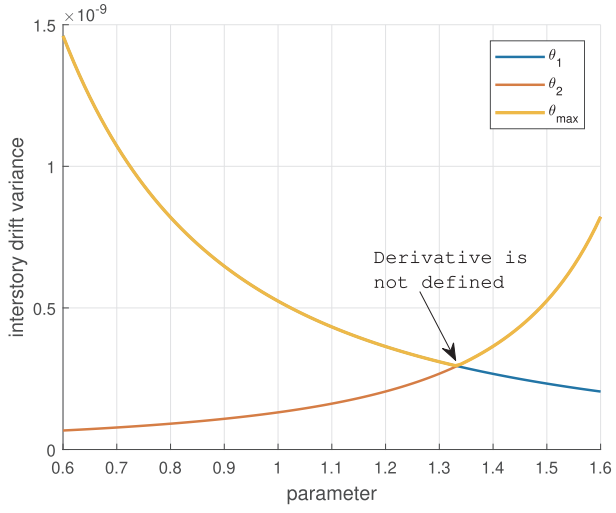

Fig. 3. Envelope function is not smooth at minimum.

elements (i.e., elements not part of the optimization domain) or lumped masses. Consequently, the structural system would be composed of a reduced number of elements with large masses, and from this assumption, model reduction can be applied to the system.

Constraints are typically applied to impose known or expected structural behavior and to reduce the number of DOF. In this study, rigid diaphragm and symmetry constraints are applied. These displacement constraints can be enforced efficiently using a transformation matrix $\mathbf{T}_c$ as follows

$$\bar{\mathbf{u}} = \mathbf{T}_c\mathbf{u} \tag{23}$$

where $\mathbf{u}$ is the vector of total DOF and $\bar{\mathbf{u}}$ is the vector of master DOF. The transformation matrix and vector of total DOF can be divided in blocks, possibly permuted due to DOF numbering, as follows

$$\mathbf{T}_c = \begin{bmatrix} \mathbf{I} \\ \mathbf{S} \end{bmatrix}, \quad \mathbf{u} = \begin{bmatrix} \bar{\mathbf{u}} \\ \mathbf{u}_c \end{bmatrix} \tag{24}$$

where $\mathbf{I}$ is the identity matrix, $\mathbf{S}$ is the constraint matrix, and $\mathbf{u}_c$ is the vector of constrained DOF. The constraint matrix $\mathbf{S}$ is a sparse matrix with exactly one non-zero entry per row and whose non-zero entries are equal to 1. Further details on the use of transformation matrix in this type of problems can be found in Gomez and Spencer [15]. Before applying the model reduction, the constraints are applied using the corresponding transformation matrix and the next discussion uses the vector of master DOF.

For model reduction, the displacement vector of the system can be divided in blocks, possibly permuted due to DOF numbering, as follows

$$\mathbf{u} = [\tilde{\mathbf{u}}^T \quad \mathbf{u}_r^T]^T \tag{25}$$

where $\tilde{\mathbf{u}}$ represents the $n_1 \times 1$ displacement vector of the few DOF that are going to be retained, where $n_1 \ll N$, and $\mathbf{u}_r$ represents the displacement vector of the removed DOF. Then, the structural matrices can be consistently divided in blocks as follows

$$\mathbf{M} = \begin{bmatrix} \mathbf{M}_{11} & \mathbf{M}_{12} \\ \mathbf{M}_{21} & \mathbf{M}_{22} \end{bmatrix}, \quad \mathbf{C} = \begin{bmatrix} \mathbf{C}_{11} & \mathbf{C}_{12} \\ \mathbf{C}_{21} & \mathbf{C}_{22} \end{bmatrix}$$
$$\mathbf{K} = \begin{bmatrix} \mathbf{K}_{11} & \mathbf{K}_{12} \\ \mathbf{K}_{21} & \mathbf{K}_{22} \end{bmatrix}, \quad \mathbf{G} = \begin{bmatrix} \mathbf{G}_1 \\ \mathbf{G}_2 \end{bmatrix} \tag{26}$$

where $\mathbf{M}_{11}$, $\mathbf{C}_{11}$, and $\mathbf{K}_{11}$ are $n_1 \times n_1$ matrices, and $\mathbf{G}_1$ is a $n_1 \times 1$ matrix.

For a undamped system in which also $\mathbf{M}_{22}$ and $\mathbf{G}_2$ are zero matrices, static condensation can be applied. However, the previous case is very restrictive. Instead the model reduction is performed using the Guyan transformation [23]

$$\mathbf{u} = \mathbf{T}\tilde{\mathbf{u}}$$
$$\mathbf{T} = \begin{bmatrix} \mathbf{I}_{n_1 \times n_1} \\ -\mathbf{K}_{22}^{-1}\mathbf{K}_{21} \end{bmatrix} \tag{27}$$

and similar relations are used for velocities and accelerations with the same transformation matrix.

The reduced system matrices can be obtained through the following well-known relations

$$\widetilde{\mathbf{M}} = \mathbf{T}^T\mathbf{M}\mathbf{T}, \quad \widetilde{\mathbf{C}} = \mathbf{T}^T\mathbf{C}\mathbf{T},$$
$$\widetilde{\mathbf{K}} = \mathbf{T}^T\mathbf{K}\mathbf{T}, \quad \widetilde{\mathbf{G}} = \mathbf{T}^T\mathbf{G} \tag{28}$$

and these matrices can be written explicitly as follows by defining $\mathbf{T}_2 = -\mathbf{K}_{22}^{-1}\mathbf{K}_{21}$

$$\widetilde{\mathbf{M}} = \mathbf{M}_{11} + \mathbf{M}_{12}\mathbf{T}_2 + \mathbf{T}_2^T\mathbf{M}_{12}^T + \mathbf{T}_2^T\mathbf{M}_{22}\mathbf{T}_2$$
$$\widetilde{\mathbf{C}} = \mathbf{C}_{11} + \mathbf{C}_{12}\mathbf{T}_2 + \mathbf{T}_2^T\mathbf{C}_{12}^T + \mathbf{T}_2^T\mathbf{C}_{22}\mathbf{T}_2$$
$$\widetilde{\mathbf{K}} = \mathbf{K}_{11} + \mathbf{K}_{12}\mathbf{T}_2$$
$$\widetilde{\mathbf{G}} = \mathbf{G}_1 + \mathbf{T}_2^T\mathbf{G}_2 \tag{29}$$

The state space representation of this reduced system and the augmented form can be obtained using the reduced system matrices, and the following small-scale Lyapunov equation can be solved to obtain the covariance of the response $\widetilde{\boldsymbol{\Gamma}}_{\mathbf{x}_a}$

$$\widetilde{\mathbf{A}}_a\widetilde{\boldsymbol{\Gamma}}_{\mathbf{x}_a} + \widetilde{\boldsymbol{\Gamma}}_{\mathbf{x}_a}\widetilde{\mathbf{A}}_a^T + 2\pi\widetilde{\mathbf{B}}_a\mathbf{S}_0\widetilde{\mathbf{B}}_a^T = \mathbf{0} \tag{30}$$

From the numerical point of view, the matrices can be obtained efficiently by using the previous equations. Moreover, this transformation reduces the size of the problem considerably, which results in a corresponding reduction in computation time for a given mesh size because only a small-scale Lyapunov equation is solved.

Although the covariance matrix $\boldsymbol{\Gamma}_{\mathbf{x}_a}$ of the initial augmented system is rarely relevant, it can be recovered from the covariance matrix $\widetilde{\boldsymbol{\Gamma}}_{\mathbf{x}_a}$ of the reduced system as follows

$$\boldsymbol{\Gamma}_{\mathbf{x}_a} = \mathbb{E}(\mathbf{x}_a\mathbf{x}_a^T) = \mathbf{T}_a\mathbb{E}(\tilde{\mathbf{x}}_a\tilde{\mathbf{x}}_a^T)\mathbf{T}_a^T = \mathbf{T}_a\widetilde{\boldsymbol{\Gamma}}_{\mathbf{x}_a}\mathbf{T}_a^T \tag{31}$$

where $\mathbf{T}_a$ is the transformation matrix for displacement and velocity. Therefore, using the specific form of the transformation matrix yields

$$\boldsymbol{\Gamma}_{\mathbf{x}_a} = \begin{bmatrix} \widetilde{\boldsymbol{\Gamma}}_{\mathbf{x}_a} & \widetilde{\boldsymbol{\Gamma}}_{\mathbf{x}_a}\mathbf{T}_{a,2}^T \\ \mathbf{T}_{a,2}\widetilde{\boldsymbol{\Gamma}}_{\mathbf{x}_a} & \mathbf{T}_{a,2}\widetilde{\boldsymbol{\Gamma}}_{\mathbf{x}_a}\mathbf{T}_{a,2}^T \end{bmatrix} \tag{32}$$

where $\mathbf{T}_{a,2}$ is the transformation matrix for displacement and velocity of the removed DOF.

3.3. Sensitivity analysis

A gradient-based optimization approach is preferred for solution of large-scale topology optimization problems for computational efficiency purposes. Critical to this approach is being able to efficiently obtain the gradients of the objective function. Previously, Gomez and Spencer [15] proposed an adjoint method to obtain the gradient of the objective function; however, this procedure cannot be applied directly for the minmax alternative formulations and they do not take advantage of the reduced-order model. Therefore, to solve these issues, the methodology is modified as shown below.

The individual objective functions J_i depend on the covariance matrix, which is implicitly defined by Eq. (30), a direct differentiation approach would be expensive due to the large number of variables. Therefore, an adjoint method is proposed, for which the following Lagrangian functions are defined with symmetric positive semidefinite Lagrange multiplier matrices $\widetilde{\boldsymbol{\Lambda}}_i$ for each objective

$$\mathcal{L}_i(\mathbf{z}, \boldsymbol{\Lambda}) = J_i(\mathbf{z}) + \widetilde{\boldsymbol{\Lambda}}_i : (\widetilde{\mathbf{A}}_a\widetilde{\boldsymbol{\Gamma}}_{\mathbf{x}_a} + \widetilde{\boldsymbol{\Gamma}}_{\mathbf{x}_a}\widetilde{\mathbf{A}}_a^T + \widetilde{\mathbf{B}}_o\widetilde{\mathbf{B}}_o^T) \tag{33}$$

where $\widetilde{\mathbf{B}}_o = \sqrt{2\pi S_0}\widetilde{\mathbf{B}}_a$. Note that the reduced-model state matrices are used in the previous definition, which leverages the use of dynamic condensation to improve efficiency.

The corresponding adjoint equations can be solved to obtain $\widetilde{\boldsymbol{\Lambda}}_i$, thus eliminating the implicitly defined gradients of $\widetilde{\boldsymbol{\Gamma}}_{\mathbf{x}_a}$,

$$\widetilde{\mathbf{A}}_a^T\widetilde{\boldsymbol{\Lambda}}_i + \widetilde{\boldsymbol{\Lambda}}_i\widetilde{\mathbf{A}}_a + \widetilde{\mathbf{F}}_i = \mathbf{0} \tag{34}$$

Eq. (34) are Lyapunov equations, which have a unique solution because $\widetilde{\mathbf{A}}_a^T$ is Hurwitz, i.e., it has eigenvalues with negative real part. Finally, the sensitivity of the functions, which are equal to the sensitivity of the Lagrangian function, are given approximately by the following equations

$$\frac{\partial J_i}{\partial z_n} = \left(\frac{\partial \widetilde{\mathbf{A}}_a}{\partial z_n}\widetilde{\boldsymbol{\Gamma}}_{\mathbf{x}_a} + \widetilde{\boldsymbol{\Gamma}}_{\mathbf{x}_a}\frac{\partial \widetilde{\mathbf{A}}_a^T}{\partial z_n} + \frac{\partial(\widetilde{\mathbf{B}}_o\widetilde{\mathbf{B}}_o^T)}{\partial z_n}\right) : \boldsymbol{\Lambda}_i + \frac{\partial \widetilde{\mathbf{F}}_i}{\partial z_n} : \widetilde{\boldsymbol{\Gamma}}_{\mathbf{x}_a} \tag{35}$$

Eq. (35) requires the gradients of the matrices $\widetilde{\mathbf{A}}_a$, $\widetilde{\mathbf{B}}_a$, and $\widetilde{\mathbf{F}}_i$ that were defined in previous sections. The detailed derivations of the results presented in this section are provided in A.

Because $\widetilde{\mathbf{F}}_i$ is symmetric positive semidefinite, the solution of the Lyapunov equation is symmetric positive semidefinite $\widetilde{\boldsymbol{\Lambda}}$, as assumed previously. Note that to compute the sensitivity of each of the functions J_i, the solution of an adjoint Lyapunov equation is required. B provides details on how solve these equations efficiently.

The examples show that the dynamic condensation provides accurate estimations of the sensitivity for the range of mass ratios of interest, and static condensation does not provide good estimations. In addition, as the mass ratio increases, the proposed method achieves better accuracy.

For the alternative formulation of the minmax problem, the sensitivity of the additional gradients is obtained directly from the gradients of the component functions, and the new objective function is linear, and its gradients are trivial. On the other hand, once the gradients of the component functions are obtained, the sensitivity of the KS function is obtained as follows

$$\frac{\partial J_{\mathrm{KS}}}{\partial z_e} = \left(\sum_{i=1}^{N_{\mathrm{f}}} e^{\rho \bar{J}_i}\right)^{-1} \left(\sum_{i=1}^{N_{\mathrm{f}}} e^{\rho \bar{J}_i} \frac{\partial J_i}{\partial z_e}\right) \tag{36}$$

3.4. Optimization details

The well-known continuous approach, based on intermediate element densities, is adopted to obtain the optimal topology [2]. For each element n, a relative density variable z_n is chosen, where $n \in \{1, 2, \ldots, N_{\mathrm{el}}\}$. Then, the Young's modulus and density for each element are obtained by some interpolation rule.

In this study, the modified Solid Isotropic Material with Penalization method (SIMP) [24,25] given by the following relationships

$$\begin{aligned} E(z) &= [\epsilon + (1-\epsilon) z^p] E^0 \\ \rho(z) &= \begin{cases} z^q \rho^0, & \text{if } z \geqslant 0.1 \\ c_0 z^{p+3} \rho^0, & \text{if } z < 0.1 \end{cases} \end{aligned} \tag{37}$$

where E and ρ are the Young's modulus and density for the element with variable z, E^0 and ρ^0 are the Young's modulus and density for the solid material, $p > 1$ and $q \geqslant 1$ are the penalization factors, ϵ is the Ersatz parameter [26], and $c_0 = 10^{p+3-q}$ is a coefficient to ensure continuity in density interpolation rule.

The solution of the proposed optimization problem is summarized in Fig. 4. In the initialization step, the domain is meshed, the element matrices using solid material are computed, the matrices for the excitation model are constructed, and the initial values for the design variables are chosen. Additionally, to avoid mesh-dependency and numerical instabilities such as checkerboard patterns and islanding, a filter is applied to the sensitivities [5]. A linear hat filter with radius R, which decreases linearly with radial distance r and is zero for $r > R$, is implemented through a filter matrix that is computed in the initialization step using centroidal distance between elements [26].

The remainder of the steps follow an iterative procedure. In the analysis step, the system matrices are obtained using the current values for the design variables, the dynamic condensation is applied to obtain a reduced system, and then, the covariance of the response is computed by solving the reduced Lyapunov equation. In the sensitivity step, the adjoint Lyapunov equations are solved to obtain the Lagrange multiplier and the performance function and constraints sensitivities; the filter is applied to the sensitivities. In the update step, the new values for the design variables are obtained by using the method of moving asymptotes [20,27]. The iterative scheme is applied until the maximum change in the design variables with respect to the previous iteration is below a specified threshold.

4. Numerical examples

First a numerical validation of the methods proposed in the previous section is performed. Then, the proposed framework is illustrated through three examples: minimization of plane buildings with 9 stories and both, single and multiple bays, and 20 stories subjected to stochastic ground motions. Geometric and dynamic properties are taken from well-known benchmark problems in structural control of buildings with seismic excitation [16].

4.1. Numerical validation

An example is performed to validate the accuracy and efficiency of the dynamic condensation to compute the stochastic response of buildings. The response is compared with the actual response obtained by solving the Lyapunov equation for the full system; and additionally, the stochastic response is also computed using static condensation to show the shortcomings this technique.

A 9-story single-bay building subjected to stochastic excitation is considered. The domain is given by the 9m × 36m rectangle, which is composed of a solid linear elastic material having the following properties, which are representative of structural steel: Young's modulus $E^0 = 200$ GPa, Poisson's ratio $\nu = 0.3$, density $\rho^0 = 7500 \frac{\mathrm{kg}}{\mathrm{m}^3}$, and Ersatz parameter $\epsilon = 10^{-4}$, which is used for the compliant material that fill the void elements. The domain has a uniform thickness of 0.25 m; and due to its thickness, the continuum domain is assumed to be in plane stress condition. The continuum domain is discretized using 36 × 144 Q4 elements. The building has 9 floors with the same height equal to 4 m. Both lateral boundaries have columns with sections that vary linearly from W14x500 to W14x257, and are discretized using 288 frame elements with axial and bending stiffness; the material properties are the same as the design domain. Additionally, there exist 18 lumped masses of magnitude M each, located on both sides of each floor. Fig. 5 shows the layout of the structure considered. Different values of M are considered independently such that $M/8000 \in \{1, 2, 5, 10, 20, 50, 100, 200\}$; one building is defined for each value of

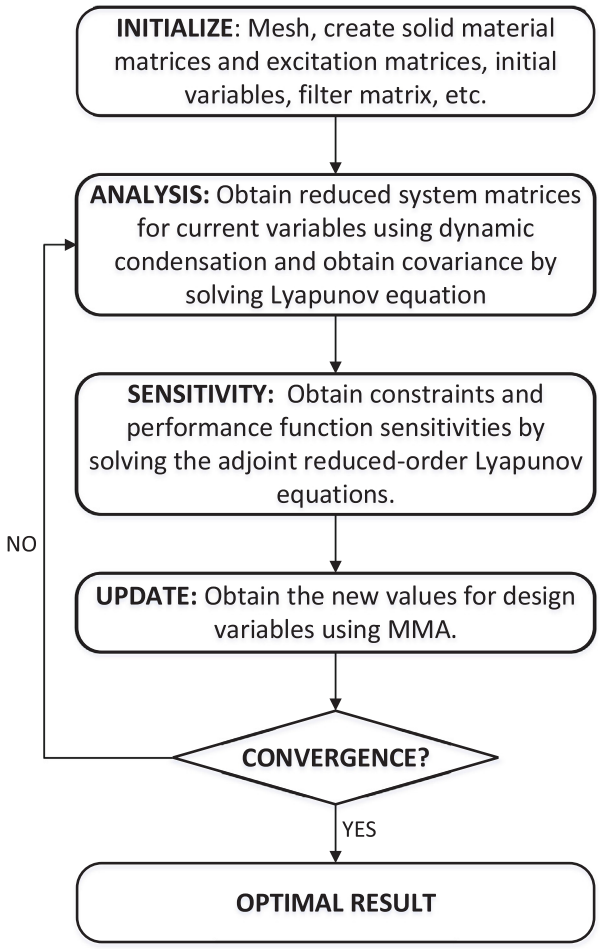

Fig. 4. Topology optimization flowchart for buildings with stochastic ground motions using dynamic condensation.

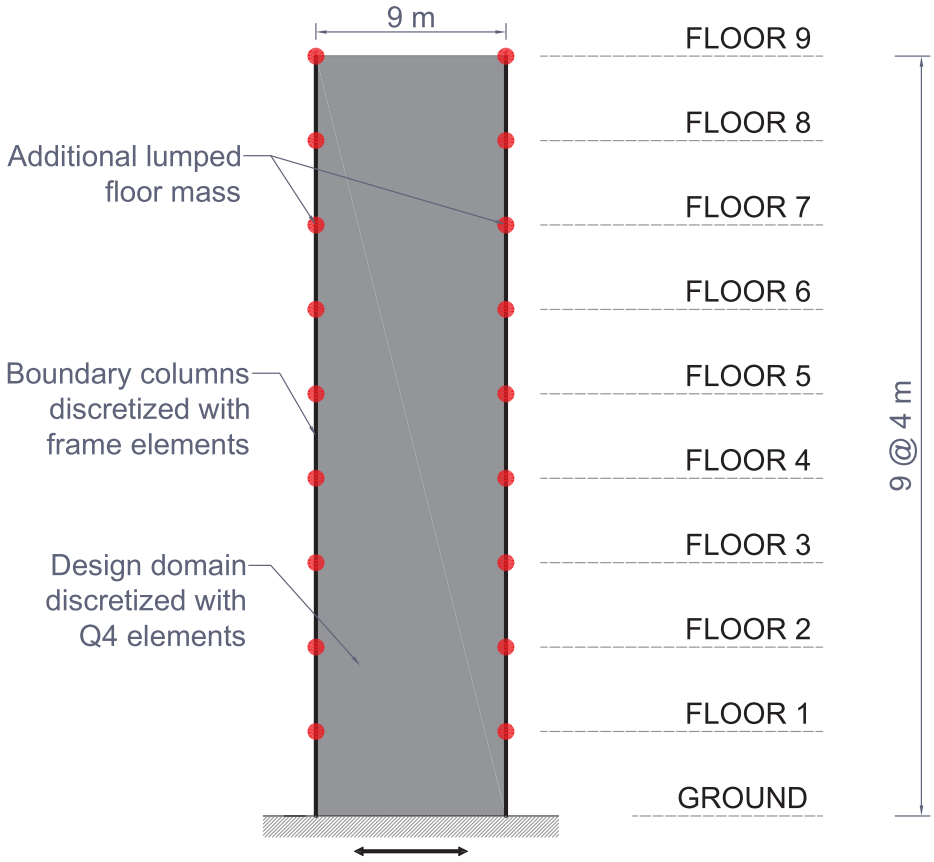

Fig. 5. 9-story single-bay building characteristics.

M. Different cases yield mass ratios μ of the retained DOF and removed DOF in the set {1, 2, 5, 10, 20, 50, 100, 200}. Pinned supports are applied to the columns and plane elements at the base. A rigid diaphragm constraint is enforced in all floors such that the joints in each floor have equal lateral displacements, i.e., representing the effect of the floor slabs. The damping matrix is obtained using Rayleigh damping with 2% damping ratio for the first two modes.

Two independent types of stochastic excitation are considered: ground motion, and equal dynamic forces on all lumped masses. In all loading cases, the excitation is modeled as a band-limited white noise (BLWN), by passing a scalar white noise (WN) with power spectral density equal to S_0 through an 8-pole, low-pass elliptic filter. The filter has a cutoff frequency 10 Hz, a peak-to-peak ripple of 0.1 dB, and stop-band attenuation of 100 dB.

The stochastic response of each structure subjected to each excitation is obtained by solving the Lyapunov equation of the complete system. In each case, the response of interest is the lateral interstory drift with covariance matrix $\mathbf{\Gamma}_0$. The proposed method using dynamic condensation retaining only the DOF with the response of interest is applied to compute the stochastic response with covariance matrix $\mathbf{\Gamma}$. To assess the accuracy of the results the following error index is defined

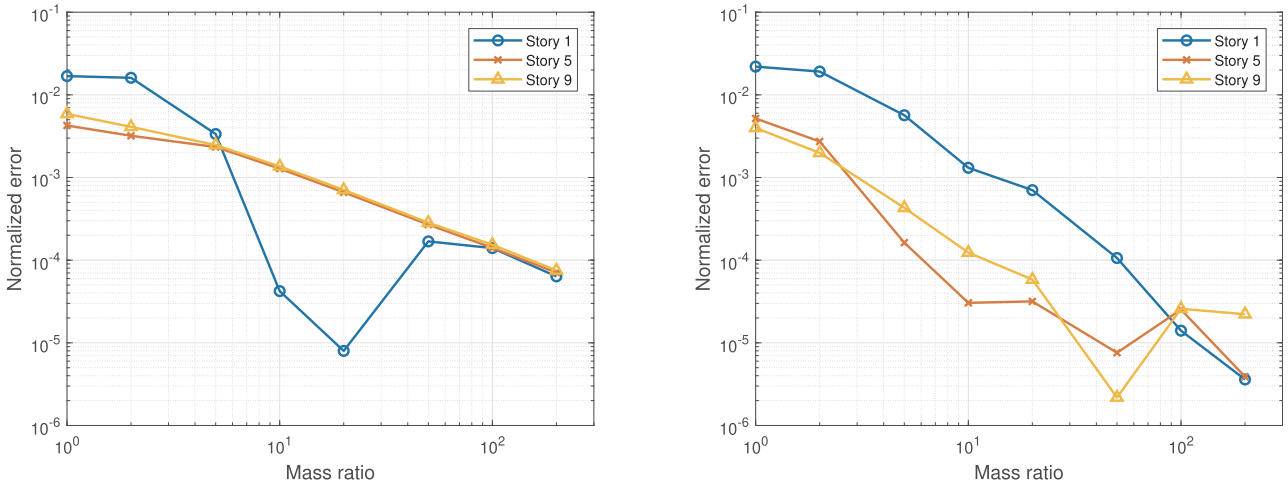

Fig. 6. Normalized error in stochastic response versus mass ratio μ for structure subjected to **(a)** ground motion and **(b)** forces in all floors.

$$e = \frac{\|\boldsymbol{\Gamma} - \boldsymbol{\Gamma}_0\|_F}{\|\boldsymbol{\Gamma}_0\|_F} \tag{38}$$

where $\|.\|_F$ represents the Frobenious norm of a matrix,i.e., the square root of the sum of the absolute squares of the matrix entries.

Fig. 6a-b show the amplitude of the error in the stochastic response versus mass ratio μ for the 2 types of excitation. The error in the stochastic response of the retained DOF using the proposed method is small for all types of excitation considered, and consequently, dynamic condensation achieves good accuracy for optimization purposes for mass ratios larger than 5.

The original problem was solved using CF-ADI algorithm with appropriate number of iterations and parameters for these type of problems [15]; a direct implementation of this solver requires a computational time of 4.9 s in a computer with processor Intel Xeon E3-1285 v6 @4.10 GHz and 32 Gb of RAM. For comparison using the same computer and the same structure, the solution using dynamic condensation requires only 0.12 s. These timing results show that the stochastic solution can be obtained for about 1/40 of the same cost of the original problem solution, which demonstrates the efficiency of the proposed approach.

This example demonstrates that dynamic condensation provides accurate and efficient estimations of the stochastic response for the range of mass ratios of interest. As the mass ratio increases, the proposed method achieves better accuracy.

To assess the accuracy of the sensitivities using dynamic condensation, the same building is considered. The value of M is set to 80 000 kg so that μ is approximately 10. Fig. 7a and Fig. 7b show the sensitivities of the variance of the interstory drift of 3 stories using the complete solution and the proposed adjoint method with dynamic condensation, respectively. Comparing both approaches, the maximum difference is less than 0.1%; and the error is expected to be lower for larger mass ratios. As these figures show, the proposed method

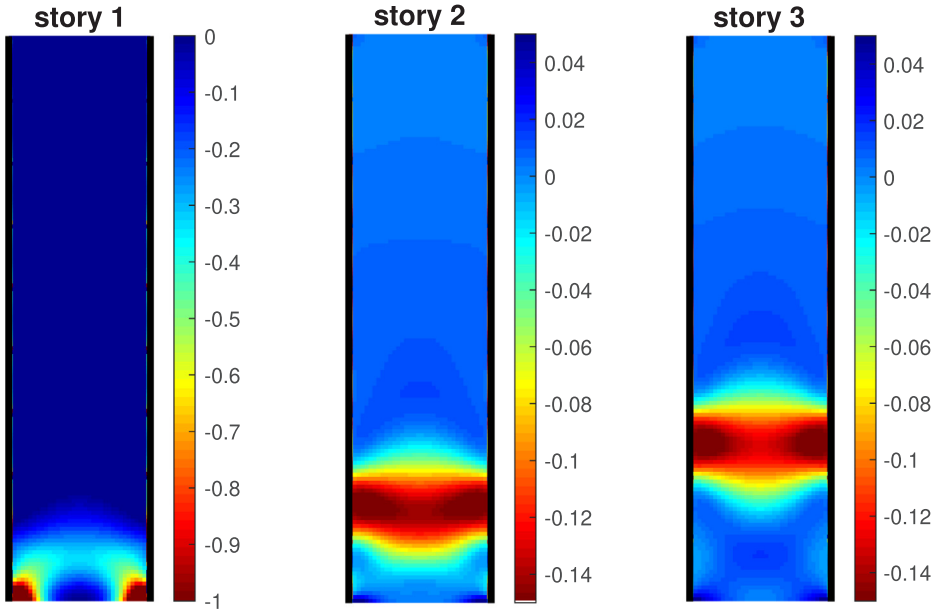

(a)

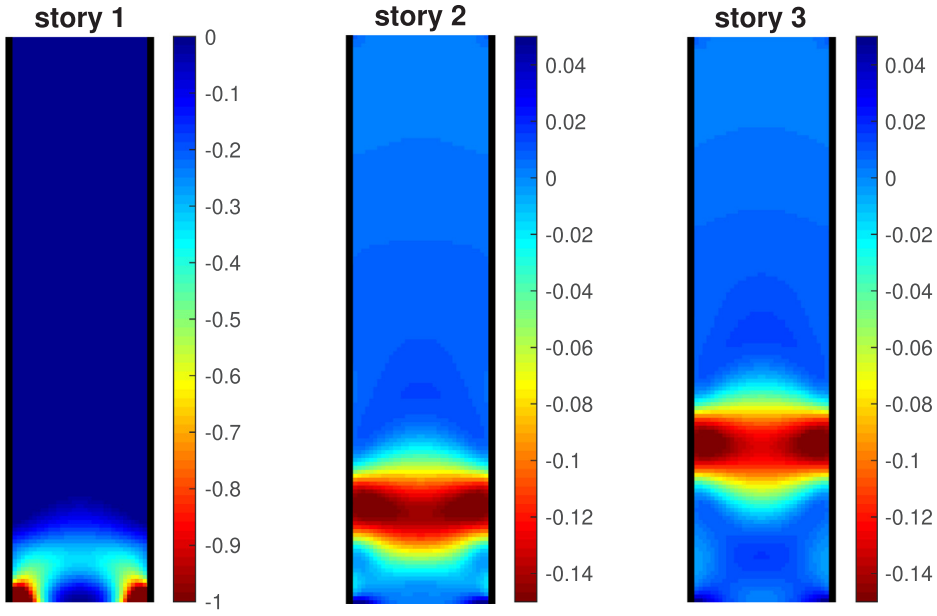

(b)

Fig. 7. Sensitivities of variance of interstory drift of 3 stories using **(a)** complete system[15] and **(b)** proposed approach using dynamic condensation.

accurately computes the sensitivities.

The sensitivities of the complete system were determined using CF-ADI algorithm and the adjoint method [15]; a direct implementation of this solver requires a computational time of 11 s in a computer with processor Intel Xeon E3-1285 v6 @4.10 GHz and 32 Gb of RAM. For comparison using the same computer and the same structure, the sensitivities using dynamic condensation require 0.45 s. These timing results show that the stochastic solution can be obtained for about 1/25 of the same cost of the original problem solution, which demonstrates the efficiency of the proposed approach.

4.2. Minimization of interstory drift for a 9-story single-bay building subjected to stochastic ground motion

In this first example, a simplified representation of the 9-story building is considered to assess the accuracy of the proposed algorithms. The general properties are taken from a single-bay in one of the North–South direction frames, from a benchmark in structural control [16]. The design domain and material properties are the same as in the example in the previous section. The domain has a uniform thickness of 0.25 m; and due to its thickness, the continuum domain is assumed to be in plane stress condition. The continuum domain is discretized using 54×216 Q4 elements. Both lateral boundaries have columns with sections W14x500 at the bottom and W14x257 at the top, and the area varies linearly for intermediate floors, the columns are discretized using 432 frame elements with axial and bending stiffness; the material properties are the same as the design domain. In addition, lumped masses of 255×10^3 kg are located in each floor and in each axis; these masses represent the structural and non-structural elements not included in the model. Pinned supports are applied to the column bases. A rigid diaphragm constraint is enforced in all floors such that the joints in each floor have equal lateral displacements. The radius of the filter is equal to 0.30 m. The volume of the optimization variables is constrained to be less or equal than 0.20 of the solid domain. The damping matrix is obtained using Rayleigh damping with 2% damping ratio for the first two modes. The optimization is performed using different objectives to compare the results and their performance.

To provide a reference of comparison, the optimal topology for minimum static compliance is obtained considering static deterministic loading forces applied to each floor level (at the lumped mass locations); the load distribution increases linearly along the height, resembling a typical first mode approximation. This optimization strategy typically resembles what in many cases is done in design offices as a simple way to determine optimal topologies for buildings subjected to seismic loads. The resulting topology is shown in Fig. 8a. The first two natural frequencies of the static design with the mass distribution described previously are equal to 1.08 Hz and 2.35 Hz. The resulting topology is 4 sets of independent X-type braces. Additional material is needed next to the columns of the first 3 floors.

Next, the ground motion $a_g(t)$ is modeled as an stochastic process using the Clough-Penzien model with $\omega_g = 15$ rad/s (2.39 Hz), $\zeta_g = 0.60$, $\omega_f = 1.5$ rad/s (0.239 Hz), $\zeta_g = 0.60$, and $S_0 = 0.026$ m^2/s^3; these parameters has been proposed for firm soil conditions [19,28] with an approximate peak ground acceleration of 0.5 times gravity. Optimization is conducted to minimize the sum of the variance of the interstory drifts (SUM objective). Fig. 8b shows the optimal design using the SUM objective; the first natural frequencies are equal to 1.05 and 2.62 Hz. Similarly to before, the resulting topology is 4 sets of independent braces with additional material needed next to the columns of the first 3 floors. Topology optimization is then performed to minimize the maximum interstory drift variance among all stories (MAX); this case is solved using bound formulation and KS function, and the results for both solutions are the same, consequently, only the result for alternative bound formulation is shown. Fig. 8c shows the optimal design for the MAX objective; the first natural frequencies are equal to 0.971 and 2.485 Hz. The resulting topology is two sets of independent braces in the first 4 floors, and some intersecting braces in the upper floors; additionally, in the first 3 floors additional material is needed next to the columns, which is equivalent to assigning bigger column sections in these floors. These figures show that the optimal topology to minimize the maximum interstory drifts differs considerably from the static design and the SUM design, although the first frequencies of these designs are relatively close to each other. Moreover, the maximum interstory drift variance in the static design, the SUM objective, and the reference design are 15.001×10^{-4} m^2, 5.245×10^{-4} m^2, and 3.323×10^{-4} m^2, respectively; which shows the superior performance of the design considering the stochastic dynamic ground motion.

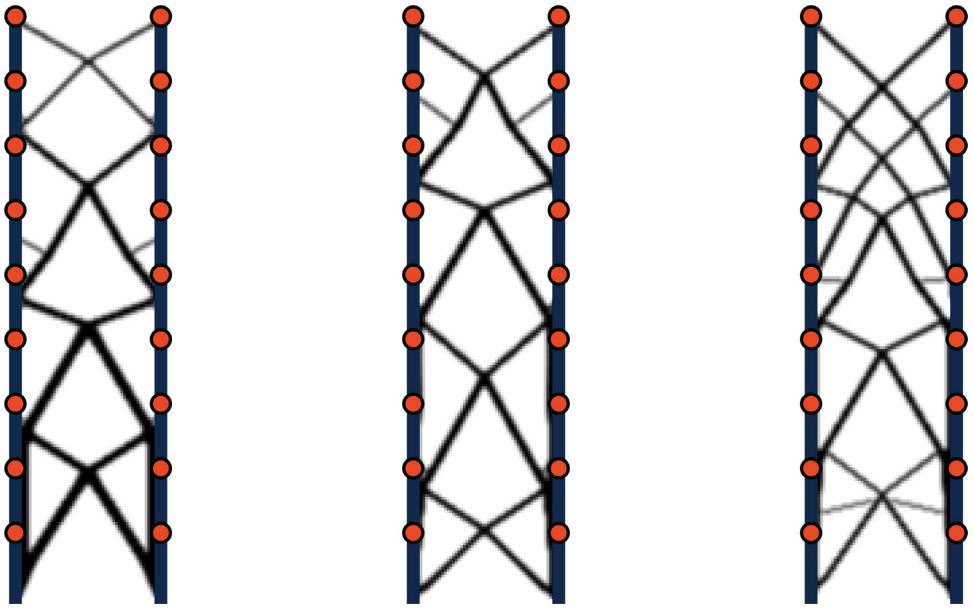

Fig. 8. Optimized topologies of 9-story single-bay building for **(a)** static compliance minimization, **(b)** minimizing the sum of interstory drift stochastic variances, and **(c)** minimizing maximum interstory drift stochastic variance.

In this example, the computational time required for each iteration using the MAX objective with the equivalent formulation is increased in 7.5% compared to the computational time using the SUM objective. This increment in computational cost is small for practical applications. The time increment occurs due to additional secondary tasks of the analysis step and sensitivity step because the Lyapunov solver already gives all the information to evaluate the objectives functions and their sensitivities. The increment of computational time for the MAX objective with the KS approximation is of the same order due to the same reasons.

Finally, the standard deviation of the interstory drift per story of the static, SUM, and MAX designs are obtained and shown in Fig. 9. The MAX objective yields a uniform distribution of interstory drifts, with the maximum value being 25% smaller than in the maximum value in the SUM objective, although in latter case, the sum of the variance of the interstory drifts is smaller. Also, the static design presents a non-uniform distribution and with values larger than the SUM and MAX designs. As expected, the MAX objective yields a design with a better performance than the other cases. The uniform distribution of interstory drift occurs for all the cases considered in this study when using the MAX objective, and this feature can be interpreted as a design with uniform damage among all floors.

4.3. Minimization of 20-story tower subjected to stochastic ground motion

The second example consists of a 20-story building subjected to ground motions. The building is also selected from the benchmarks for control problems [16]. Similarly to the previous example, only one frame in the North–South direction is considered here for the optimization. The general properties are slightly modified from the original problem and they are described next.

The design domain is given by the 30 m × 80 m rectangle, which is composed of a solid linear elastic material having the properties of structural steel. The domain has a uniform thickness of 0.10 m; and due to its thickness, the continuum domain is assumed to be in plane stress condition. The continuum domain is discretized using 90×240 Q4 elements. The building has 20 floors with the same height equal to 4 m and 5 bays with a span of 6 m. Both lateral boundaries have columns with sections W24x335 at the bottom and W24x84 at the top, and the area varies linearly for intermediate floors, the columns are discretized using 1440 frame elements with axial and bending stiffness; the material properties are the same as the design domain. In addition, lumped masses of 46×10^3 kg are located in each floor and in each axis; these masses represent the structural and non-structural elements not included in the model. Pinned supports are applied to the column bases. Two types of axial stiffness are considered in all floors: rigid diaphragm constraints such that the nodes in each floor have equal lateral displacements, and a flexible diaphragm with axial stiffness provided by floor beams W30x108. The radius of the filter is equal to 0.50 m. The volume of the optimization variables is constrained to be less or equal than 0.30 of the solid domain. The damping matrix is obtained using Rayleigh damping with 2% damping ratio for the first two modes. The objective is to minimize the maximum interstory drift among all stories. For the case with flexible diaphragms, the interstory drift is computed as the average of the relative displacement with respect to the previous floor at each column axis.

Two independent ground motions $a_g(t)$ are considered using Clough-Penzien model for different soil conditions, whose parameters are shown in Table 1; these parameters have been proposed for medium and firm soil conditions, respectively [19,28]. For both excitations $S_0 = 0.026\ \text{m}^2/\text{s}^3$. Topology optimization is performed to minimize the maximum interstory drift variance among all stories for each ground motion.

Fig. 10a-b show the optimal design for both excitations with rigid diaphragms; the first natural frequencies of the first design are equal to 1.20 Hz and 2.96 Hz, and the first natural frequencies of the second design are equal to 1.18 Hz and 3.16 Hz. The maximum interstory drift variance in both designs are $0.645 \times 10^{-4}\ \text{m}^2$ and $0.434 \times 10^{-4}\ \text{m}^2$, respectively; which shows that the first excitation is more severe because the peak frequency of the excitation is closer to the first frequency of the structure. These figures show that the optimal topology differs locally for the different excitations. In both designs, a mega bracing pattern resembling a beam emerges with some local and global bracing to restraint the floor masses. In both cases, the interstory drift distribution is uniform for all 20 floors.

Fig. 11a-b show the optimal design for both excitations with flexible diaphragms; the first natural frequencies of the first design are equal to 1.16 Hz and 2.85 Hz, and the first natural frequencies of the second design are equal to 1.14 Hz and 2.96 Hz. The maximum interstory drift variance in both designs are $0.679 \times 10^{-4}\ \text{m}^2$ and $0.455 \times 10^{-4}\ \text{m}^2$, respectively; which again shows that the first excitation is more severe because the peak frequency of the excitation is closer to the first frequency of the structure. Likewise, these figures show that the optimal topology differ locally for the different excitations. These results indicate that the topology is highly dependent in the type of diaphragm; a rigid diaphragm results in a simpler layout, and a flexible diaphragm results in a structure with more local braces that also provides local axial stiffness in each floor.

To assess the robustness to parameter changes in ground motions, the distribution of the standard deviation of the interstory drifts of two designs are computed for each ground motion; Fig. 12a-b display these results for the designs with flexible diaphragms. The distribution of interstory drifts in both designs is uniform for the excitation it was designed for, and this result provides a good indicator that the design is near or at the optimum. Additionally, the optimal result for medium soil performs well for the ground motion of firm soil and vice versa, which indicates the robustness of the designs to variations in the ground motion parameters. Similar conclusions were obtained for the rigid diaphragm designs.

5. Conclusions

This paper proposed an efficient topology optimization framework for building subjected to stochastic ground motions. The solution of large-scale Lyapunov equations is time consuming, and typically, in

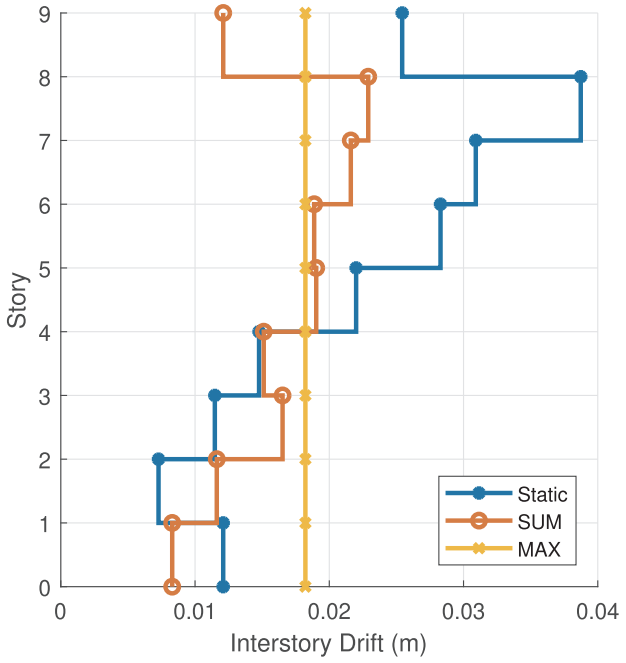

Fig. 9. Comparison of the distribution of interstory drift standard deviation for static compliance, SUM, and MAX designs.

Table 1
Parameters of the ground excitation model for different soil conditions [19,28].

Soil type	ω_g	ζ_g	ω_f	ζ_f
Medium soil	10 rad/s (1.59 Hz)	0.4	1.0 rad/s (0.159 Hz)	0.6
Firm soil	15 rad/s (2.39 Hz)	0.6	1.5 rad/s (0.239 Hz)	0.6

buildings only the response of a few points, i.e. floor nodes, is of interest. Consequently, the system matrices were reduced using a Guyan reduction transformation, from which a small-scale Lyapunov equation was solved to obtain the stationary response covariances of the floors. This approach to obtain the stochastic response of retained degrees-of-freedom was verified for multiple examples with different additional-mass-to-structural-mass ratio, which demonstrated that the accuracy is excellent for ratios larger than 5 and that computational time efficiency is considerably improved.

In addition, this study considered more realistic details in the topology optimization of stochastically excited buildings such as additional floor masses, gravity boundary elements, diaphragm constraints, and ground motion stochastic models. Also, the performance function was given by the maximum covariance among the floor responses, which yields a non-differentiable problem near to the maximum response point in the design domain. Therefore, two alternative smooth formulations were proposed to fix this issue: bound formulation and using the KS function approximation of the envelope. The first approach introduces an additional variable, additional smooth constraints, and a new smooth objective function. Details on how to evaluate the new constraints were also discussed.

A volume constraint was imposed to limit the design space, and the design variables were chosen as the relative densities in each element, which were bounded to achieve physically meaningful solutions. The material properties for intermediate densities were obtained using the SIMP interpolation rule; a linear hat filter was used to avoid numerical instabilities. In addition, an efficient adjoint method was developed to obtain the sensitivities of the performance function and additional functions, which required the solution of an additional small-scale Lyapunov equation. The proposed approach to obtain the sensitivities was compared with other methods, which demonstrated good agreement in the results. Iterations were carried out using a gradient-based approach commonly employed in the topology optimization field.

The proposed topology optimization scheme is illustrated for two planar frames of buildings with 9 stories single-bay, and 20 stories 5 bays. The building characteristics were taken from well-known benchmark problems in structural control of building subjected to ground motions. The lateral resisting system in each example was designed to minimize the maximum interstory drift among all stories. The first example optimized the lateral resisting system of a 9-story and single-bay building. The system was optimized for the static compliance case, the sum of variance of interstory drifts, and the maximum variance of interstory drifts. The static deterministic loads were applied on the lumped masses with a linear variation over height approximating the

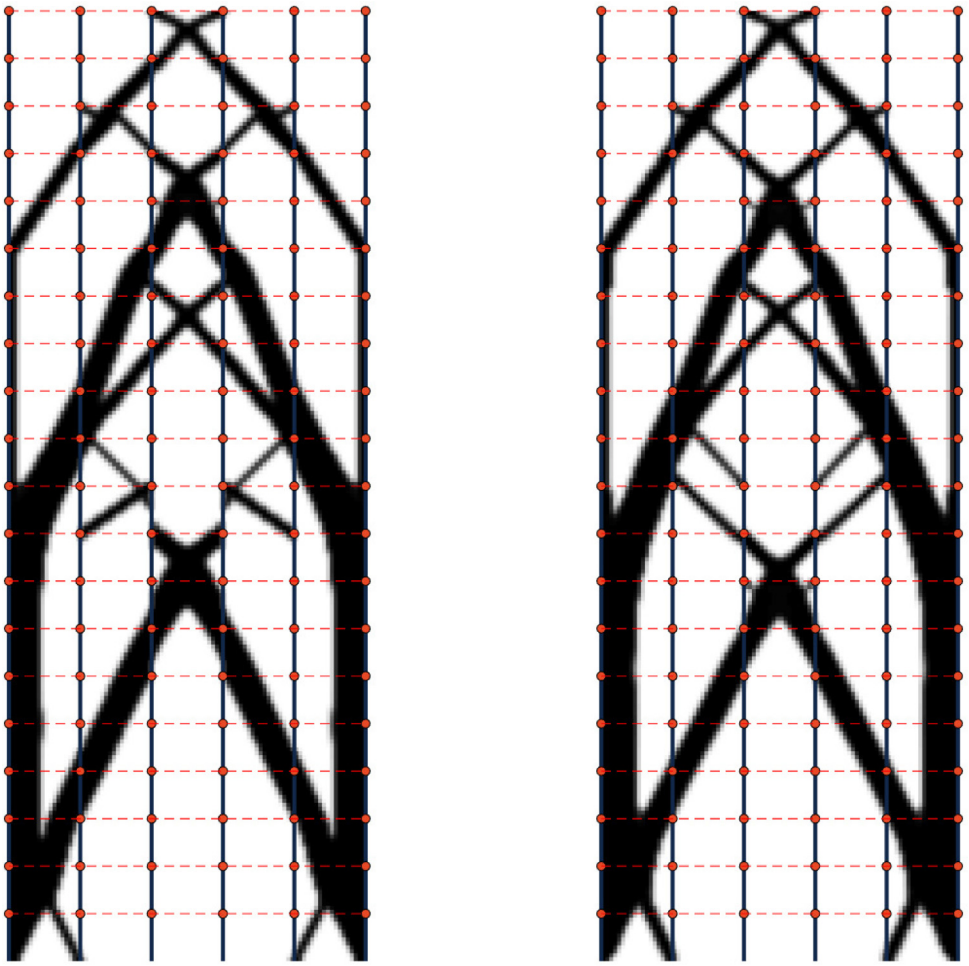

(a) (b)

Fig. 10. Optimized topologies for minimizing maximum interstory drift stochastic variance with a rigid diaphragm at each floor subjected to ground motion with **(a)** medium soil (ω_g = 10 rad/s) and **(b)** firm soil (ω_g = 15 rad/s).

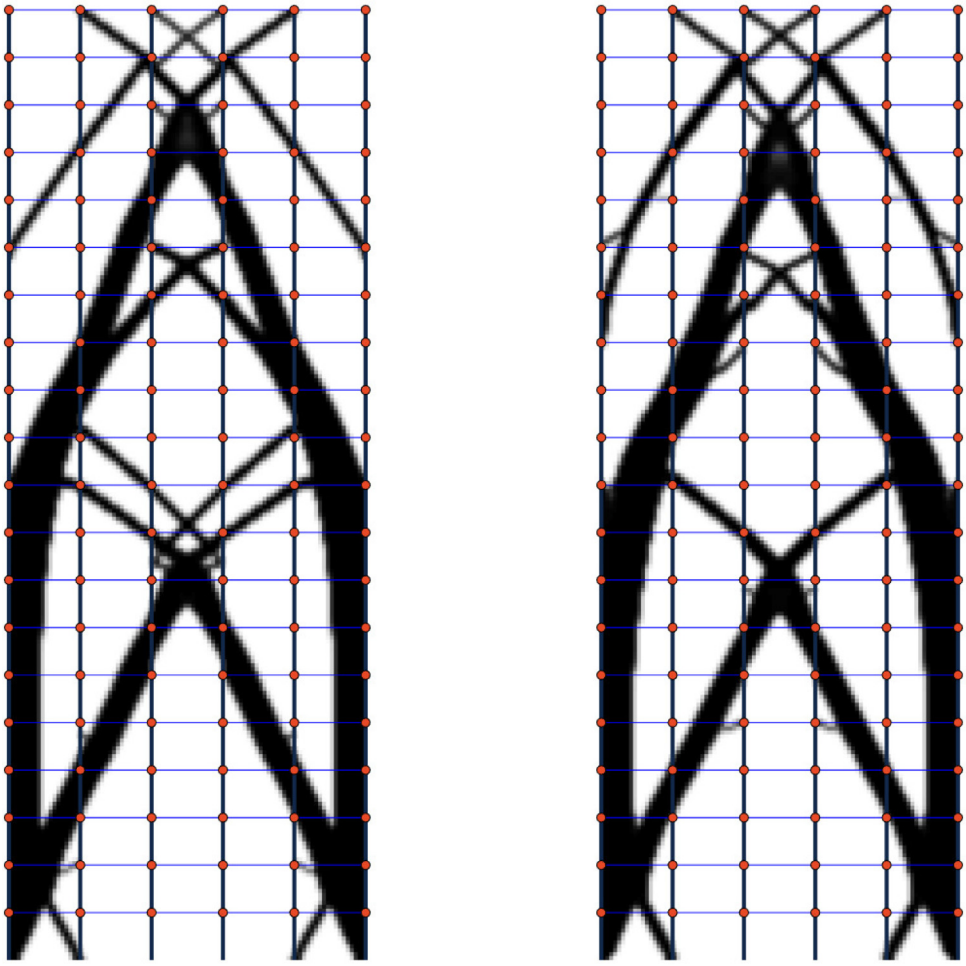

(a) (b)

Fig. 11. Optimized topologies for minimizing maximum interstory drift stochastic variance with a flexible diaphragm at each floor subjected to ground motion with **(a)** medium soil (ω_g = 10 rad/s) and **(b)** firm soil (ω_g = 15 rad/s).

first mode and the proposed method achieved superior performance. The different objectives yielded different results, and the response to the stochastic ground motion of each design was obtained. It was demonstrated that the MAX objective achieved a different topology with a reduced maximum response, the static case yielded the worse response. Moreover, using the MAX objective, a uniform distribution of interstory drift variance was obtained, and a non-uniform distribution for the other objectives.

The second example optimized the lateral resisting system of a 20-story and 5-bay building. The design was performed for a set of parameters given by the benchmark problem with 2 different excitations and 2 different diaphragm types. The design consisted of a mega bracing spanning multiple floors with internal and external bracing patterns restraining the lumped masses. The topology is highly dependent in the type of diaphragm, and changing the excitation parameters modified local details of the topology because of the change in the excitation peak frequency, but the optimal design seems to be robust to changes in the excitation parameters. In all cases, a uniform distribution of interstory drift variance was obtained.

The results presented herein demonstrate the efficiency of the proposed approach for topology optimization of buildings excited by ground motions, which presents a useful tool for designers to explore new types of structural patterns in earthquake-prone areas. This framework can be extended to accommodate multi-objective problems as well as multiple input-multiple output systems.

CRediT authorship contribution statement

Fernando Gomez: Conceptualization, Methodology, Software, Formal analysis, Investigation, Writing - original draft, Writing - original draft, Writing - review & editing, Visualization. **Billie F. Spencer Jr.:** Conceptualization, Methodology, Resources, Writing - review & editing. **Juan Carrion:** Conceptualization, Methodology, Writing - review & editing.

Declaration of Competing Interest

None.

Declaration of Competing Interest

The authors declare that they have no known competing financial interests or personal relationships that could have appeared to influence the work reported in this paper.

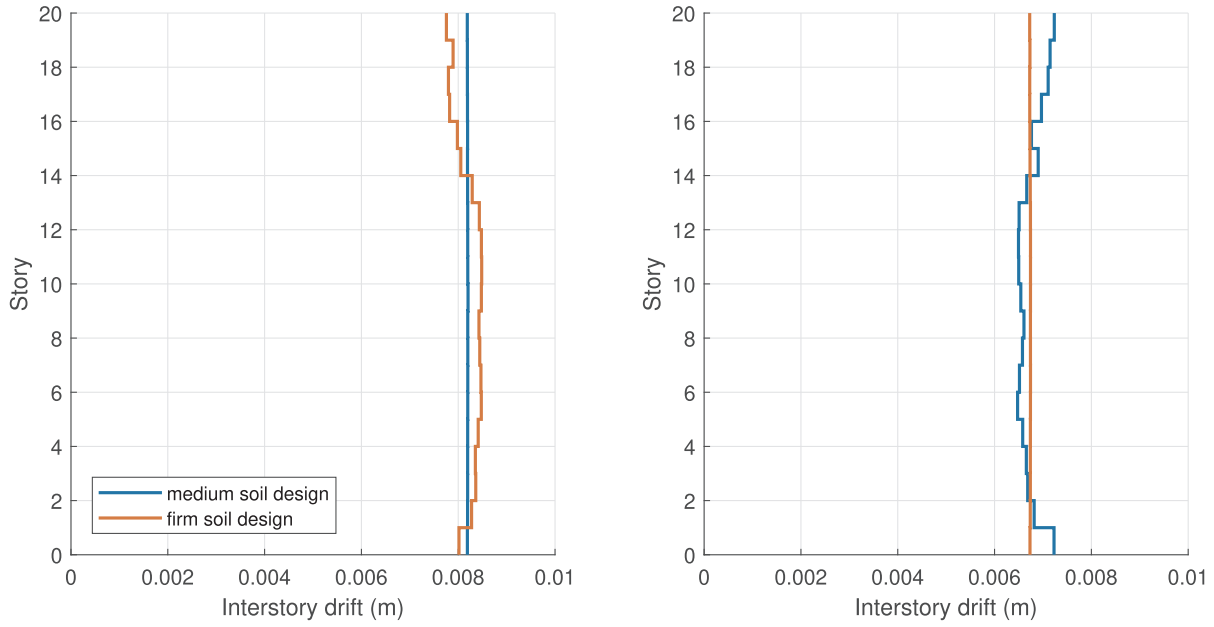

Fig. 12. Comparison of the distribution of interstory drift stochastic standard deviation for designs with flexible diaphragm due to ground motion for **(a)** medium soil and **(b)** firm soil.

Appendix A. Sensitivity analysis

The details on how to obtain the sensitivity of the performance functions described in Section 3.3 are described in this section. Initial notation is used and the subscript of the covariance of the response of the augmented system is dropped for simplicity; and the indices take values from 1, 2, ...,N' unless noted otherwise. Direct differentiation method requires the solution of one Lyapunov equation for each element, which makes the overall process a quartic order process. An adjoint method is applied to make the process more efficient, in terms of the Lagrangian functions expressed in Eq. (33), which is rewritten and reordered next in initial notation

$$\mathcal{L}_p = J_p + \Lambda_{p,ij}(\widetilde{A}_{\mathrm{a},ik}\widetilde{\Gamma}_{kj} + \widetilde{\Gamma}_{ik}\widetilde{A}_{\mathrm{a},jk} + Q_{ij}) = J_p + (\widetilde{\mathrm{A}}_{\mathrm{a},ki}\widetilde{\Lambda}_{\mathrm{p},kj} + \widetilde{\Lambda}_{\mathrm{p},ik}\widetilde{\mathrm{A}}_{\mathrm{a},kj})\widetilde{\Gamma}_{ij} + \widetilde{\Lambda}_{\mathrm{p},ij}\mathrm{Q}_{ij} \tag{39}$$

where $\mathbf{Q} = \widetilde{\mathbf{B}}_{\mathrm{o}}\widetilde{\mathbf{B}}_{\mathrm{o}}^{\mathrm{T}}$. Differentiating the previous equation yields the following

$$\frac{\partial \mathcal{L}_p}{\partial z_n} = \frac{\partial J_p}{\partial z_n} + \frac{\partial(\widetilde{A}_{\mathrm{a},ki}\widetilde{\Lambda}_{p,kj} + \widetilde{\Lambda}_{p,ik}\widetilde{A}_{\mathrm{a},kj})}{\partial z_n}\widetilde{\Gamma}_{ij} + (\widetilde{A}_{\mathrm{a},ki}\widetilde{\Lambda}_{p,kj} + \widetilde{\Lambda}_{p,ik}\widetilde{A}_{\mathrm{a},kj})\frac{\partial \widetilde{\Gamma}_{ij}}{\partial z_n} + \widetilde{\Lambda}_{p,ij}\frac{\partial Q_{ij}}{\partial z_n} \tag{40}$$

Plugging the derivative of the function J_i in the previous equation and reordering yields

$$\frac{\partial \mathcal{L}_p}{\partial z_n} = \frac{\partial(\widetilde{A}_{\mathrm{a},ki}\widetilde{\Lambda}_{p,kj} + \widetilde{\Lambda}_{p,ik}\widetilde{A}_{\mathrm{a},kj})}{\partial z_n}\widetilde{\Gamma}_{ij} + \widetilde{\Lambda}_{p,ij}\frac{\partial Q_{ij}}{\partial z_n} + (\widetilde{A}_{\mathrm{a},ki}\widetilde{\Lambda}_{p,kj} + \widetilde{\Lambda}_{p,ik}\widetilde{A}_{\mathrm{a},kj} + \widetilde{F}_{p,ij})\frac{\partial \widetilde{\Gamma}_{ij}}{\partial z_n} + \frac{\partial \widetilde{F}_{p,ij}}{\partial z_n} \tag{41}$$

To remove the dependence on the implicit derivative of the covariance matrix, the first factor in the third term in the RHS of the previous equation is defined as 0, that is

$$\widetilde{A}_{\mathrm{a},ki}\widetilde{\Lambda}_{p,kj} + \widetilde{\Lambda}_{p,ik}\widetilde{A}_{\mathrm{a},kj} + \widetilde{F}_{p,ij} = 0 \tag{42}$$

which written in abstract form yields Eq. (20). Therefore, the gradient of the performance function is given by

$$\frac{\partial J_p}{\partial z_n} = \left(\frac{\partial \widetilde{A}_{\mathrm{a},ik}}{\partial z_n}\widetilde{\Gamma}_{kj} + \widetilde{\Gamma}_{ik}\frac{\partial \widetilde{A}_{\mathrm{a},jk}}{\partial z_n} + \frac{\partial Q_{ij}}{\partial z_n}\right)\widetilde{\Lambda}_{p,ij} + \frac{\partial F_{p,ij}}{\partial z_n} \tag{43}$$

and the previous equation written in abstract form gives Eq. (35).

Then, the sensitivity of the performance function requires the derivatives of the matrices $\widetilde{\mathbf{A}}_{\mathrm{a}}$ and $\widetilde{\mathbf{B}}_{\mathrm{a}}$, these are obtained similarly to the derivatives of the state matrices of the total system [15] but using the reduced-order matrices derivatives, which are shown next for the ease of the reader

$$\frac{\partial \widetilde{\mathbf{A}}_{\mathrm{a}}}{\partial z_n} = \begin{bmatrix} \frac{\partial \widetilde{\mathbf{A}}_{\mathrm{s}}}{\partial z_n} & \frac{\partial \widetilde{\mathbf{B}}_{\mathrm{s}}}{\partial z_n}\mathbf{C}_{\mathrm{f}} \\ \mathbf{0}_{N_1\times 2n_1} & \mathbf{0}_{N_1\times N_1} \end{bmatrix}, \quad \frac{\partial \widetilde{\mathbf{B}}_{\mathrm{a}}}{\partial z_n} = \mathbf{0} \tag{44}$$

The derivative of state matrices are given by

$$\frac{\partial \widetilde{\mathbf{A}}_{\mathrm{s}}}{\partial z_n} = \begin{bmatrix} \mathbf{0}_{n_1\times n_1} & \mathbf{0}_{n_1\times n_1} \\ \frac{\partial(-\widetilde{\mathbf{M}}^{-1}\widetilde{\mathbf{K}})}{\partial z_n} & \frac{\partial(-\widetilde{\mathbf{M}}^{-1}\widetilde{\mathbf{C}})}{\partial z_n} \end{bmatrix} \tag{45}$$

$$\frac{\partial \widetilde{\mathbf{B}}_{\mathrm{s}}}{\partial z_n} = \begin{bmatrix} \mathbf{0}_{n_1 \times 1} \\ \frac{\partial (\widetilde{\mathbf{M}}^{-1}\widetilde{\mathbf{G}})}{\partial z_n} \end{bmatrix} \tag{46}$$

and the following derivatives that appear in the state matrices are given by

$$\begin{aligned} \frac{\partial(-\widetilde{\mathbf{M}}^{-1}\widetilde{\mathbf{K}})}{\partial z_n} &= \widetilde{\mathbf{M}}^{-1}\left(\frac{\partial \widetilde{\mathbf{M}}}{\partial z_n}\widetilde{\mathbf{M}}^{-1}\widetilde{\mathbf{K}} - \frac{\partial \widetilde{\mathbf{K}}}{\partial z_n}\right) \\ \frac{\partial(-\widetilde{\mathbf{M}}^{-1}\widetilde{\mathbf{C}})}{\partial z_n} &= \widetilde{\mathbf{M}}^{-1}\left(\frac{\partial \widetilde{\mathbf{M}}}{\partial z_n}\widetilde{\mathbf{M}}^{-1}\widetilde{\mathbf{C}} - \frac{\partial \widetilde{\mathbf{C}}}{\partial z_n}\right) \\ \frac{\partial(-\widetilde{\mathbf{M}}^{-1}\widetilde{\mathbf{G}})}{\partial z_n} &= \widetilde{\mathbf{M}}^{-1}\left(-\frac{\partial \widetilde{\mathbf{M}}}{\partial z_n}\widetilde{\mathbf{M}}^{-1}\widetilde{\mathbf{G}} + \frac{\partial \widetilde{\mathbf{G}}}{\partial z_n}\right) \end{aligned} \tag{47}$$

If Rayleigh damping is used, the damping matrix is equal to

$$\widetilde{\mathbf{C}} = \alpha_1 \widetilde{\mathbf{M}} + \alpha_2 \widetilde{\mathbf{K}} \tag{48}$$

and consequently, the derivative of this matrix is computed from this relationship. If there is an additional source of damping, similar relations as the previous ones can be obtained for the derivative of the damping matrix; however, in many cases the damping matrix due to supplemental damping is not dependent on the densities, and therefore, its derivative is zero. From the previous expression, the following derivative is given by

$$\frac{\partial(-\widetilde{\mathbf{M}}^{-1}\widetilde{\mathbf{C}})}{\partial z_n} = \alpha_2 \widetilde{\mathbf{M}}^{-1}\left(\frac{\partial \widetilde{\mathbf{M}}}{\partial z_n}\widetilde{\mathbf{M}}^{-1}\widetilde{\mathbf{K}} - \frac{\partial \widetilde{\mathbf{K}}}{\partial z_n}\right) \tag{49}$$

The matrices $\mathbf{M}$ and $\mathbf{K}$ are obtained using an assembly process described by

$$\mathbf{M}(\mathbf{z}) = \sum_{n=1}^{N_{\mathrm{el}}} \rho(z_n)\mathbf{M}_n^0, \quad \mathbf{K}(\mathbf{z}) = \sum_{n=1}^{N_{\mathrm{el}}} E(z_n)\mathbf{K}_n^0 \tag{50}$$

where $\mathbf{M}_n^0$ and $\mathbf{K}_n^0$ are the mass and stiffness matrices of element n with solid material in global DOF. The derivatives of them are given by

$$\frac{\partial \mathbf{M}}{\partial z_n} = \frac{\partial \rho}{\partial z}(z_n)\mathbf{M}_n^0, \quad \frac{\partial \mathbf{K}}{\partial z_n} = \frac{\partial E}{\partial z}(z_n)\mathbf{K}_n^0 \tag{51}$$

Then the derivatives of the matrices can be split in blocks as follows

$$\frac{\partial \mathbf{M}}{\partial z_n} = \begin{bmatrix} \frac{\partial \mathbf{M_{11}}}{\partial z_n} & \frac{\partial \mathbf{M_{12}}}{\partial z_n} \\ \frac{\partial \mathbf{M_{21}}}{\partial z_n} & \frac{\partial \mathbf{M_{22}}}{\partial z_n} \end{bmatrix}, \quad \frac{\partial \mathbf{K}}{\partial z_n} = \begin{bmatrix} \frac{\partial \mathbf{K_{11}}}{\partial z_n} & \frac{\partial \mathbf{K_{12}}}{\partial z_n} \\ \frac{\partial \mathbf{K_{21}}}{\partial z_n} & \frac{\partial \mathbf{K_{22}}}{\partial z_n} \end{bmatrix}, \quad \frac{\partial \mathbf{G}}{\partial z_n} = \begin{bmatrix} \frac{\partial \mathbf{G_1}}{\partial z_n} \\ \frac{\partial \mathbf{G_2}}{\partial z_n} \end{bmatrix} \tag{52}$$

Then, the following derivative is obtained

$$\frac{\partial \mathbf{T_2}}{\partial z_n} = \mathbf{K_{22}^{-1}}\frac{\partial \mathbf{K_{22}}}{\partial z_n}\mathbf{K_{22}^{-1}}\mathbf{K_{21}} - \mathbf{K_{22}^{-1}}\frac{\partial \mathbf{K_{21}}}{\partial z_n} \tag{53}$$

and the derivatives of the reduced-order matrices are as follows

$$\begin{aligned} \frac{\partial \widetilde{\mathbf{M}}}{\partial z_n} =& \frac{\partial \mathbf{M_{11}}}{\partial z_n} + \frac{\partial \mathbf{M_{12}}}{\partial z_n}\mathbf{T_2} + \mathbf{M_{12}}\frac{\partial \mathbf{T_2}}{\partial z_n} + \frac{\partial \mathbf{T_2^T}}{\partial z_n}\mathbf{M_{12}^T} + \mathbf{T_2^T}\frac{\partial \mathbf{M_{12}^T}}{\partial z_n} \\ &+ \frac{\partial \mathbf{T_2^T}}{\partial z_n}\mathbf{M_{22}}\mathbf{T_2} + \mathbf{T_2^T}\frac{\partial \mathbf{M_{22}}}{\partial z_n}\mathbf{T_2} + \mathbf{T_2^T}\mathbf{M_{22}}\frac{\partial \mathbf{T_2}}{\partial z_n} \\ \frac{\partial \widetilde{\mathbf{K}}}{\partial z_n} =& \frac{\partial \mathbf{K_{11}}}{\partial z_n} + \frac{\partial \mathbf{K_{12}}}{\partial z_n}\mathbf{T_2} + \mathbf{K_{12}}\frac{\partial \mathbf{T_2}}{\partial z_n} \\ \frac{\partial \widetilde{\mathbf{G}}}{\partial z_n} =& \frac{\partial \mathbf{G_1}}{\partial z_n} + \frac{\partial \mathbf{T_2}}{\partial z_n}^{\mathrm{T}}\mathbf{G_2} + \mathbf{T_2^T}\frac{\partial \mathbf{G_2}}{\partial z_n} \end{aligned} \tag{54}$$

Appendix B. Multiple Lyapunov equation solution

Because of the proposed method to solve the minimax problem and the adjoint method to obtain sensitivities, multiple adjoint Lyapunov equations of the following form need to be solved

$$\widetilde{\mathbf{A}}_{\mathrm{a}}^{\mathrm{T}}\widetilde{\mathbf{\Lambda}}_i + \widetilde{\mathbf{\Lambda}}_i\widetilde{\mathbf{A}}_{\mathrm{a}} + \widetilde{\mathbf{F}}_i = \mathbf{0} \tag{55}$$

Because of the dynamic condensation approach, the number of DOFs is reduced, but application of previous algorithms to obtain the solution may still require excessive time if many constraints are introduced. Fortunately, existing algorithms can be modified to solve this problem efficiently; in this section modifications to Bartel-Stewards and CF-ADI algorithms, for small and large-scale equations, respectively, are described.

The solution of the Lyapunov equation using the Bartels-Steward algorithm requires the Schur factorization of the matrix $\widetilde{\mathbf{A}}_{\mathrm{a}}$, which needs to be done only once because it is the same state matrix for all equations. Then, each equation is converted to a Lyapunov equation with quasi-triangular matrices and they can be solved as usual. Doing the factorization only once yields time savings because it is the most expensive step in the solution of the Lyapunov equation.

The solution using CF-ADI algorithm first requires the computation of the optimal shift parameters, which depend only in $\widetilde{\mathbf{A}}_{\mathrm{a}}$; therefore, these parameters need to be obtained only once $\widetilde{\mathbf{A}}_{\mathrm{a}}$. Because each of the matrices $\widetilde{\mathbf{F}}_i = \mathbf{C}_i^{\mathrm{T}}\mathbf{C}_i$, then the following matrix is defined

$$\mathbf{C}_{\mathrm{t}} = [\mathbf{C}_1^{\mathrm{T}} \;\; \mathbf{C}_2^{\mathrm{T}} \;\; \ldots \;\; \mathbf{C}_{n'}^{\mathrm{T}}]^{\mathrm{T}} \tag{56}$$

and

$$\mathbf{F}_t = \mathbf{C}_t^T \mathbf{C}_t \tag{57}$$

It is easily shown that

$$\mathbf{F}_t = \widetilde{\mathbf{F}}_1 + \widetilde{\mathbf{F}}_2 + ... + \widetilde{\mathbf{F}}_{n'} \tag{58}$$

Applying the CF-ADI algorithm to solve the following low-rank sparse Lyapunov equation

$$\widetilde{\mathbf{A}}_a^T \widetilde{\mathbf{\Lambda}}_i + \widetilde{\mathbf{\Lambda}}_i \widetilde{\mathbf{A}}_a + \mathbf{F}_t = \mathbf{0} \tag{59}$$

yields the complex matrix $\mathbf{Z}$

$$\mathbf{Z} = [\mathbf{V}_1 \quad \mathbf{V}_2 \quad ... \quad \mathbf{V}_n] \tag{60}$$

where the matrices $\mathbf{V}_i$ are obtained using an iterative procedure. Finally, the Lagrange multipliers can be obtained as follows

$$\widetilde{\mathbf{\Lambda}}_i = \mathbf{Z}_i \mathbf{Z}_i^H \tag{61}$$

where ^{H} denotes the Hermitian transpose operation and $\mathbf{Z}_i$ is the matrix composed of columns of the matrices $\mathbf{V}_i$, using as many columns and in the same order as the rows of $\mathbf{C}_i$ in $\mathbf{C}_t$. By solving the multiple Lyapunov equations as proposed, the total time for the solution is the same as in the SOV case, which is considerably more efficient than solving large-scale Lyapunov equations many times.

References

[1] Xu J, Spencer BF, Lu X, Chen X, Lu L. Optimization of structures subject to stochastic dynamic loading. Comput-Aided Civil Infrastruct Eng 2017;32:657–73.
[2] Bendsøe MP, Sigmund O. Topology optimization: theory, methods, and applications. Springer; 2003.
[3] Bendsøe MP, Kikuchi N. Generating optimal topologies in structural design using a homogenization method. Comput Methods Appl Mech Eng 1988;71:197–224.
[4] Bendsøe MP, Sigmund O. Material interpolation schemes in topology optimization. Arch Appl Mech (Ingenieur Archiv) 1999;69:635–54.
[5] Sigmund O, Petersson J. Numerical instabilities in topology optimization: A survey on procedures dealing with checkerboards, mesh-dependencies and local minima. Struct Optim 1998;16:68–75.
[6] Díaz A, Sigmund O. Checkerboard patterns in layout optimization. Struct Optim 1995;10:40–5.
[7] Sigmund O. Morphology-based black and white filters for topology optimization. Struct Multidiscip Optim 2007;33:401–24.
[8] Soong TT, Grigoriu M. Random vibration of mechanical and structural systems. PTR Prentice Hall; 1993.
[9] Balling RJ, Balling LJ, Richards PW. Design of buckling-restrained braced frames using nonlinear time history analysis and optimization. J Struct Eng 2009;135:461–8.
[10] Allahdadian S, Boroomand B. Topology optimization of planar frames under seismic loads induced by actual and artificial earthquake records. Eng Struct 2016;115:140–54.
[11] Chun J, Song J, Paulino GH. Structural topology optimization under constraints on instantaneous failure probability. Struct Multidiscipl Optim 2016;53:773–99.
[12] Zhang WH, Liu H, Gao T. Topology optimization of large-scale structures subjected to stationary random excitation: An efficient optimization procedure integrating pseudo excitation method and mode acceleration method. Comput Struct 2015;158:61–70.
[13] Zhu M, Yang Y, Guest JK, Shields MD. Topology optimization for linear stationary stochastic dynamics: Applications to frame structures. Struct Saf 2017;67:116–31.
[14] Hu Z, Ma H, Su C. Topology optimization of structures subjected to non-stationary random excitations. In: International symposium on sustainability and resiliency of infrastructure, Taipei, Taiwan.
[15] Gomez F, Spencer BF. Topology optimization framework for structures subjected to stationary stochastic dynamic loads. Struct Multidiscip Optim 2019;59:813–33.
[16] Ohtori Y, Christenson RE, Spencer BF, Dyke SJ. Benchmark control problems for seismically excited nonlinear buildings. J Eng Mech 2004;130:366–85.
[17] Stromberg LL, Beghini A, Baker WF, Paulino GH. Topology optimization for braced frames: Combining continuum and beam/column elements. Eng Struct 2012;37:106–24.
[18] Kanai K. Semi-empirical Formula for the Seismic Characteristics of Ground. Trans Archit Inst Japan 1957;57(1):281–4.
[19] Clough RW, Penzien J. Dynamics of structures, McGraw-Hill, New York: 2nd ed.; 1993.
[20] Svanberg K. The method of moving asymptotes—a new method for structural optimization. Int J Numer Meth Eng 1987;24:359–73.
[21] Bendsøe MP, Olhoff N, Taylor JE. A variational formulation for multicriteria structural optimization*. J Struct Mech 1983;11:523–44.
[22] James KA, Hansen JS, Martins JR. Structural topology optimization for multiple load cases using a dynamic aggregation technique. Eng Optim 2009;41:1103–18.
[23] Craig RR, Kurdila A. Fundamentals of structural dynamics. John Wiley; 2006.
[24] Tcherniak D. Topology optimization of resonating structures using SIMP method. Int J Numer Meth Eng 2002;54:1605–22.
[25] Du J, Olhoff N. Topological design of freely vibrating continuum structures for maximum values of simple and multiple eigenfrequencies and frequency gaps. Struct Multidiscip Optim 2007;34:91–110.
[26] Talischi C, Paulino GH, Pereira A, Menezes IFM. PolyTop: a Matlab implementation of a general topology optimization framework using unstructured polygonal finite element meshes. Struct Multidiscip Optim 2012;45:329–57.
[27] Svanberg K. A class of globally convergent optimization methods based on conservative convex separable approximations. SIAM J Optim 2002;12:555–73.
[28] Kiureghian AD, Neuenhofer A. Response spectrum method for multi-support seismic excitations. Earthquake Eng Struct Dynam 1992;21:713–40.